

Global and regional radiative forcing from 20% reductions in BC, OC and SO₄ - an HTAP2 multi-model study

Camilla Weum Stjern¹, Bjørn Hallvard Samset¹, Gunnar Myhre¹, Huisheng Bian², Mian Chin³, Yanko Davila⁴, Frank Dentener⁵, Louisa Emmons⁶, Johannes Flemming⁸, Amund Søvde Haslerud¹, Daven Henze⁴, Jan Eiof Jonson⁷, Tom Kucsera⁹, Marianne Tronstad Lund¹, Michael Schulz⁷, Kengo Sudo¹⁰, Toshihiko Takemura¹¹, Simone Tilmes⁶

¹ CICERO Center for International Climate and Environmental Research, Oslo, Norway

² Goddard Earth Sciences and Technology Center, University of Maryland, Baltimore, Maryland, USA

³ Earth Sciences Division, NASA Goddard Space Flight Center, Greenbelt, MD, USA

⁴ Department of Mechanical Engineering, University of Colorado, Boulder, CO, USA

⁵ European Commission, Joint Research Centre, Institute for Environment and Sustainability, Ispra (VA), Italy

⁶ Atmospheric Chemistry Division, National Center for Atmospheric Research (NCAR), CO, USA

⁷ Norwegian Meteorological Institute, Oslo, Norway

⁸ European Centre for Medium Range Weather Forecast (ECMWF), Reading, UK

⁹ Universities Space Research Association, Greenbelt, MD, USA

¹⁰ Nagoya University, Furocho, Chigusa-ku, Nagoya, Japan

¹¹ Research Institute for Applied Mechanics, Kyushu University, Fukuoka, Japan

Correspondence to: Camilla W. Stjern (camilla.stjern@cicero.oslo.no)

Abstract

In the Hemispheric Transport of Air Pollution Phase 2 (HTAP) exercise, a range of global atmospheric general circulation and chemical transport models performed coordinated perturbation experiments with 20 % reductions in emissions of anthropogenic aerosols, or aerosol precursors, in a number of source regions. Here, we compare the resulting changes in the atmospheric load and vertically resolved profiles of black carbon (BC), organic aerosols (OA) and sulfate (SO₄) from 10 models that include treatment of aerosols. We use a set of temporally, horizontally and vertically resolved profiles of aerosol forcing efficiency (AFE) to estimate the impact of emission changes in six major source regions on global radiative forcing (RF) pertaining to the direct aerosol effect, finding values between 51.9 and 210.8 mWm⁻² Tg⁻¹ for BC, between -2.4 and -17.9 mWm⁻² Tg⁻¹ for OA, and between -3.6 and -10.3 Wm⁻² Tg⁻¹ for SO₄. In most cases, the local influence dominates, but results show that mitigations in South and East Asia have substantial impacts on the radiative budget in all investigated receptor regions, especially for BC. In Russia and the Middle East, more than 80 % of the forcing for BC and OA is due to extra-regional emission reductions. Similarly, for North America, BC emissions control in East Asia is found to be more important than domestic mitigations, which is consistent with previous findings. Comparing fully resolved RF calculations to RF estimates based on vertically averaged AFE profiles allows us to quantify the importance of vertical resolution to RF estimates. We find that locally in the source regions, a 20 % emission reduction strengthens the radiative forcing associated with SO₄ by 25 % when including the vertical dimension, as the AFE for SO₄ is strongest near the surface. Conversely, the local RF from BC weakens by 37 % since BC AFE is low close to the ground. The fraction of BC direct effect forcing attributable to inter-continental transport, on the

44 other hand, is enhanced by one third when accounting for the vertical aspect, because long-range
45 transport primarily leads to aerosol changes at high altitudes, where the BC AFE is strong. While the
46 surface temperature response may vary with the altitude of aerosol change, the analysis in the present
47 study is not extended to estimates of temperature or precipitation changes.

48 **1. Introduction**

49 Atmospheric aerosols have a range of effects on the atmosphere, biosphere and on human beings.
50 They significantly alter the global radiative balance, through processes spanning from direct
51 interaction with sunlight (Myhre et al., 2013; Yu et al., 2006) to modification of cloud properties
52 (Lohmann and Feichter, 2005; Stevens and Feingold, 2009) and influences on thermal stability (Koch
53 and Del Genio, 2010). Aerosols have also been shown to affect regional precipitation (Liu et al., 2011;
54 Khain, 2009) and atmospheric circulation patterns (Bollasina et al., 2011). In addition to climatic
55 impacts come the adverse effects that aerosol pollution has on human health (Janssen, 2012; Geng et
56 al., 2013). Changes in aerosol emissions are therefore of interest both for climate and public health
57 policies (Shindell et al., 2012), which makes it imperative to provide precise estimates of aerosol
58 effects on these outcomes. However, present day emissions have high spatial and temporal variability,
59 and acquiring accurate measurements is a challenge. Similarly, aerosol atmospheric lifetimes and
60 processes leading to long-range transport are insufficiently quantified. The total anthropogenic aerosol
61 radiative forcing (RF) since the onset of the industrial period counters large parts of the positive RF
62 from CO₂ and other greenhouse gases, and was recently evaluated to be -0.9 W m^{-2} with a 95 %
63 uncertainty interval from -1.9 to -0.1 W m^{-2} (Boucher et al., 2013). Of the total aerosol RF, the direct
64 short-wave aerosol radiative interaction contributed with -0.35 W m^{-2} , with an uncertainty interval of
65 -0.85 to $+0.15 \text{ W m}^{-2}$. These large uncertainty intervals imply that the RF from aerosols is poorly
66 constrained. Likewise, there is still a large divergence between model- and satellite-derived surface
67 particulate matter and observed concentrations (Brauer et al., 2016).

68 One specific uncertainty in calculating aerosol RF is connected to the vertical distribution of aerosols.
69 The radiative impact of an aerosol depends on its absorbing and reflecting properties, but these
70 properties, as well as their radiative impact, are subject to modifications by variable atmospheric
71 conditions. For instance, relative humidity has a large impact on the scattering properties of light
72 reflecting aerosols (Fierz-Schmidhauser et al., 2010; Haywood and Shine, 1997). Also, the radiative
73 forcing efficiency of absorbing aerosols is augmented with increasing quantities of underlying clouds
74 and gases that reflect solar radiation back onto the aerosols, thereby enhancing their absorption
75 (Zarzycki and Bond, 2010). Meanwhile, competition with other processes such as Rayleigh scattering
76 and radiative interactions of other aerosol species (Samset and Myhre, 2011) may dampen the
77 radiative impact of an aerosol. As these factors typically vary with altitude, so will the aerosols'
78 forcing efficiency. Accurate knowledge of the vertical distribution of aerosol load is therefore
79 important (Ban-Weiss et al., 2012; Samset and Myhre, 2015; Vuolo et al., 2014; Zarzycki and Bond,
80 2010). Presently, the atmospheric models that simulate the climate impact of aerosols have substantial
81 variations in their vertical distribution of aerosols. In fact, results from the recent AeroCom Phase II
82 multimodel exercise (Samset et al., 2014; Samset et al., 2013) show that differences in vertical profiles
83 gave rise to between 20 % and 50 % of the intermodel differences in direct RF estimated from
84 common BC emissions from fossil fuel and biofuels (FF+BF).

85 Due to long-range atmospheric transport, emissions in major source regions may have widespread
86 health and climate impacts that go far beyond the domestic domain. Studies of long-range transport of
87 aerosols have found that the vertical distribution of aerosols in the source region has important

88 implications to the magnitude and spatial extent of their climate impact – not only because of the
89 variation of forcing efficiency with height, but because the strong large-scale winds in the upper
90 troposphere can transport aerosols for particularly long distances if they reach these levels. For
91 instance, Liu et al. (2008) found in a study of Cloud-Aerosol Lidar and Infrared Pathfinder Satellite
92 Observations (CALIPSO) measurements that the higher Saharan dust aerosols were lifted up in the
93 source region, the further they were carried across the Atlantic Ocean. Similarly, Huang et al. (2008)
94 studied long-range transport from Asia during the Pacific Dust Experiment (PACDEX) and found
95 indications of aerosol transport via upper tropospheric westerly jets – the efficiency of which was
96 influenced by the vertical distribution of Asian dust in the free troposphere of the source region.

97 These studies underline the need for a better understanding of how variations between atmospheric
98 models contribute to the uncertainties in radiative forcing estimates, and specifically the role of
99 different vertical distribution of aerosols to these uncertainties. In 2005, the Task Force on
100 Hemispheric Transport of Air Pollution (TF HTAP) was established under the United Nations
101 Economic Commission for Europe (UNECE) Convention on Long- Range Transboundary Air
102 Pollution (LRTAP Convention). One of its goals is to further our understanding of aerosol
103 intercontinental transport, and assess impacts of emission changes on air quality, climate, and
104 ecosystems (<http://www.htap.org/>). The climate impact of aerosol emission reductions in four large
105 source regions was investigated for a series of model simulations from the first phase of the HTAP
106 Task Force (HTAP1) by Yu et al. (2013), who calculated radiative forcing as the product between
107 aerosol optical depth and an aerosol forcing efficiency (AFE) estimated using the Goddard Chemistry
108 Aerosol Radiation and Transport (GOCART) model. They found that when all anthropogenic
109 emissions were reduced by 20 % in North America, Europe, South Asia or East Asia, the four-region
110 average global direct radiative forcing of SO₄, particulate organic matter and black carbon was
111 lowered about 9 %, 3 % and 10 %, respectively. Together, the four-region total emissions accounted
112 for 72 %, 21 % and 46 % of global emissions for SO₄, particulate organic matter and black carbon,
113 respectively. Inter-model differences were found to be substantial, in part because the models were
114 using different emission inventories in their simulations.

115 The present study utilizes model experiments organized by the second phase of the TF HTAP
116 (HTAP2). We focus on the six priority source regions (Fig. 1) selected by the TF HTAP for HTAP2:
117 North America (NAM), Europe (EUR), South Asia (SAS), East Asia (EAS),
118 Russia/Belarusia/Ukraine (RUS) and the Middle East (MDE). Note that while the first four regions
119 are similar to those investigated by Yu et al. (2013), the HTAP2 regions are defined by geopolitical
120 boundaries while the HTAP1 regions were larger and included more ocean areas. We aim to explain
121 how much a 20 % emission reduction in these source regions would impact other regions in terms of
122 aerosol burden and radiative forcing changes. To estimate the climate impacts of the mitigations we
123 calculate radiative forcing based on column averaged aerosol fields and AFE estimates in a method
124 equivalent to Yu et al. (2013) (here, using the OsloCTM2 model), but we extend the analyses to also
125 involve 4D AFE and aerosol burden profiles. This allows us to quantify how the vertical distribution
126 of aerosols influences the potential impact of regional emission mitigation strategies.

127 Previous studies have shown that the relationship between instantaneous BC RF, which is what we
128 estimate here, and the resulting surface temperature change also depends on the altitude of the BC.
129 The dependence is however not the same as for instantaneous RF. Although not found in all studies
130 (Ming et al., 2010), indications are that near the surface BC causes strong warming, through the
131 middle of the troposphere it is only weakly warming, whereas near the tropopause and in the
132 stratosphere, BC may even cause surface cooling (Ban-Weiss et al., 2012; Samset and Myhre, 2015;
133 Sand et al., 2013a; Shindell and Faluvegi, 2009). The difference is related both to the indirect and

134 semi-direct impacts of BC on clouds, both of which cause negative RF, due, respectively, to
135 microphysical impacts on cloud albedo, and changes in cloud cover due to alterations in atmospheric
136 stability and relative humidity. It is beyond the scope of this study to calculate climate change in terms
137 of surface temperature change, and we stress that a positive/negative estimate of direct RF here should
138 not be translated directly into warming or cooling.

139 In the next section, we will go through our methods. Section 3 presents the results, starting with
140 changes in aerosol concentrations for the different experiments, and moving on to resulting changes in
141 radiative forcing as well as the influence of inter-continental transport. The results are summarized in
142 Sect. 4.

143 **2. Methods**

144 **2.1 The HTAP2 experiments and models**

145 As part of the HTAP2 exercise, global aerosol-climate CTMs and GCMs performed a baseline (*BASE*)
146 simulation with climate and aerosol emissions corresponding to present day (year 2010) conditions
147 (Galmarini, 2016). Anthropogenic emissions followed Janssens-Maenhout et al. (2015), which for
148 year 2010 give global BC, OC and SO₂ emissions of 5.56, 12.58 and 106.47 Tg species/year,
149 respectively. Each model also ran simulations with all anthropogenic emissions reduced by 20 % in a
150 selection of source regions. We have chosen to focus on the six priority source regions pointed out by
151 the TF HTAP and shown in Fig. 1 (a). The experiments where all anthropogenic emissions are reduced
152 by 20 % in the NAM, EUR, SAS, EAS, RBU and MDE regions are referred to correspondingly as
153 *NAMreduced*, *EURreduced*, *SASreduced*, *EASreduced*, *RBUreduced* and *MDEreduced*. We will
154 additionally analyze emission reduction influences on the Arctic, also marked in Fig. 1 (a).

155 The present study takes input from ten global aerosol models, listed in Table 1 along with core
156 parameters and references. Horizontal and vertical resolutions of the models are also indicated in
157 Table 1. The time resolution of output used in this study is monthly for all models, although models
158 were run at finer resolution. To be included here, we required that the models had provided 3D,
159 temporally resolved mass mixing ratios of atmospheric aerosols for both the baseline and at least four
160 of the reduced emission scenarios. All models used prescribed meteorology for the year 2010.
161 Obviously, the use of one specific year will impact the results as prevailing wind patterns and
162 precipitation levels in the different source regions will vary from year to year, which will influence
163 transport and removal processes. For instance, 2010 marked the beginning of the strong 2010-2012 La
164 Niña event, which has been shown to be associated with above-normal intensities of the Asian
165 monsoon (Goswami and Xavier, 2005).

166 The analyzed aerosol species include sulfate (SO₄), organic aerosols (OA) and black carbon (BC). A
167 limitation of the current analyses of OA is that while some models reported OA directly, others gave
168 emissions and concentrations of OC instead (see Table S-1). OC can be converted to OA through
169 multiplication by an OC-to-OA conversion factor, which varies with source, aerosol age and the
170 presence of other chemical species (see e.g. Tsigaridis et al. (2014) and references therein). However,
171 due to limited level of detail in the available model data, as well as due to consistency to the method
172 used in Chin et al. (manuscript in preparation), we multiplied all OC values by a factor 1.8 to obtain
173 OA. As some of the models have included secondary organic aerosols (SOA) in their OA values while
174 other have not, this approximation likely leads to additional inter-model variability.

175 Model output was provided as mass mixing ratio (MMR, unit of $\mu\text{g}/\text{kg}$), but we have also analyzed the
176 data in terms of column integrated aerosol abundance. The conversion from MMR to column
177 abundance was done by interpolating the MMR fields from each model to the resolution of one host
178 model (OsloCTM2) with a vertical resolution of 60 layers, using pressure and mass of air distributions
179 from that model and summing over all layers. See e.g. Samset et al. (2013) for a detailed description of
180 this method.

181

182 **2.2 Estimating radiative forcing**

183 None of the participating models performed native RF calculations. In order to estimate the radiative
184 forcing resulting from the emission and subsequent concentration reductions simulated by the HTAP2
185 experiments, we therefore utilized precalculated 4D distributions of aerosol forcing efficiency (AFE),
186 which is defined as the RF per gram of a given aerosol species. For the three aerosol species, AFE was
187 calculated for each grid cell and month by inserting a known amount of aerosol within a known
188 background of aerosols and clouds, for each model layer individually, and calculating the resulting
189 radiative effect using an 8-stream radiative transfer model (Stamnes et al., 1988) with four short wave
190 spectral bands (Myhre et al., 2009). I.e. the model was used to calculate the response to a change in
191 aerosol concentration at a given altitude, and run for a whole year to capture seasonal variability. The
192 simulations for different model layers were then combined into a set of radiative kernels, one for each
193 aerosol species. For the radiative transfer calculations aerosol optical properties were derived from
194 Mie theory. The absorption of aged BC was enhanced by 50% to take into account external mixing, as
195 suggested by Bond and Bergstrom (2006), and for all models we assume the same mixing ratio
196 between aged and non-aged BC as in OsloCTM2. Hygroscopic growth of SO_4 was included, scaling
197 with relative humidity according to Fitzgerald (1975). See Myhre et al. (2004) and Myhre et al. (2007)
198 for a discussion on the impacts of this choice. For OA, purely scattering aerosols are assumed.
199 Background aerosols were taken from simulations using OsloCTM2. See Samset and Myhre (2011)
200 for details, but note that all numbers have been updated since that work, taking into account recent
201 model improvements (Samset and Myhre, 2015). The resulting AFE profiles, averaged over the
202 individual regions from Fig. 1 (a), is presented in Sect. 3.3. For a full discussion on the impact on
203 radiative forcing from using a single model kernel, see Samset et al. (2013). Briefly, multi-model
204 average forcing becomes representative of that of the host model, including cloud fields and optical
205 properties, while the variability around this value is indicative of the impact of differences in 3D
206 aerosol burdens. The resulting reduction in multi-model relative standard deviation depends on the
207 regional and vertical differences in AFE, but is generally less than 20%.

208 The direct RF from a given aerosol species due to a 20 % emission reduction was then estimated by
209 multiplying the modelled aerosol burden change profile ΔBD (from a given HTAP2 model and
210 experiment) with the OsloCTM2 AFE distribution for that species and point in space and time (month
211 of the year):

$$212 \quad RF(lon, lat, lev, time) = \Delta BD(lon, lat, lev, time) \times AFE(lon, lat, lev, time) \quad (1)$$

213 The RF calculated at each model level using this method should be interpreted as the instantaneous
214 radiative forcing exerted at top of the atmosphere (TOA), due to the aerosol abundance within that
215 layer.

216 As mentioned above, using this procedure means that intermodel variability will likely be lower than if
217 the models had provided their own estimates of RF, and that the absolute RF will be influenced by the

218 mean efficiency of the host model (OsloCTM2). As recently shown in the AeroCom Phase II model
 219 intercomparison (Myhre et al., 2013), OsloCTM2 is among the models with strongest global, annual
 220 mean AFE values for BC and OA, in part due to the heightened complexity of the radiation scheme
 221 used (Myhre and Samset, 2015). For SO₄, the AFE of OsloCTM2 is close to the AeroCom median.

222
 223 Validation of these kernel estimates against natively calculated RF was not possible in this analysis, as
 224 no RF values were available from the model groups. However, Samset et al. (2013) performed a
 225 comparison between model simulated and kernel estimated RF and found that for BC, between 20 and
 226 50% of the variability could be attributed to vertical BC profiles alone, with the rest being due to a
 227 combination of optical properties, horizontal transport and differences in cloud fields. Also note that
 228 Stier et al. (2013) investigated model uncertainty in direct RF for twelve AeroCom models and found
 229 substantial diversity in both clear- and all-sky RF even when aerosol radiative properties were
 230 prescribed.

231 As will be shown below, there are significant differences between the vertical profiles of aerosol
 232 abundance predicted by the participating models. To estimate the effect of these differences on global,
 233 annual mean RF, we also compute the radiative forcing in a way that does not account for the vertical
 234 aerosol distributions: we average out the vertical dimension by calculating column aerosol burdens
 235 and multiply by corresponding full column AFE distributions from OsloCTM2, which utilized the
 236 specific vertical aerosol distribution of that model.

$$237 \quad RF_{3D}(lon, lat, time) = \Delta BD(lon, lat, time) \times AFE(lon, lat, time) \quad (2)$$

238 Here, RF_{3D} indicates a radiative forcing estimate where the two horizontal dimensions, as well as
 239 time, is included, but where the vertical dimension is averaged out. For further details on the above
 240 method, see Samset et al. (2013).

241

242 **2.3 Response to extra-regional emission reductions**

243 The impact of intercontinental transport between regions is investigated through calculating the
 244 Response to Extra-Regional Emission Reductions (RERER). While this metric is originally defined in
 245 HTAP (2010) to study the influence of inter-continental transport on region average burden change or
 246 surface concentrations, we utilize a version of the RERER defined in HTAP (2010) studying instead
 247 the influence on forcing:

$$248 \quad RERER_{sr} = \frac{\Delta RF_{base,global} - \Delta RF_{base,sr}}{\Delta RF_{base,global}} = \frac{(RF_{base} - RF_{global}) - (RF_{base} - RF_{sr})}{RF_{base} - RF_{global}} \quad (3)$$

249 Here, *base* refers to the base simulation with no emission reductions, *global* refers to an experiment
 250 where anthropogenic emissions all over the globe are reduced by 20 %, and *sr* refers to the experiment
 251 where emissions in source region *sr* are reduced by 20 %. RERER is then calculated for all source
 252 regions and species. A low RERER value means that the forcing within a region is not very sensitive
 253 to extra-regional emission reductions.

254 In addition to the above calculation of RERER for RF, we also calculate RERER for changes in total
 255 column aerosol burden, which gives an estimate of inter-continental transport in two dimensions
 256 (ignoring the vertical).

257

258 3. Results and discussion

259 In the following sections, we first present the global and regional aerosol burdens simulated by the
260 participating models in response to the baseline emissions, before moving on to showing the local and
261 remote burden changes due to 20 % reduction in regional emissions. Then, we show the calculated
262 radiative forcing from these burden changes, and discuss how regional aerosol mitigation efforts may
263 impact local and remote regions.

264 3.1 Baseline aerosol burdens and emissions

265 Figures 1 (b) – (d) show the multi-model median column integrated burden fields for BC, OA and
266 SO₄, respectively, for the unperturbed *BASE* simulation. The source regions of focus in this study are
267 mostly recognized as regions of high aerosol burden in the maps, as are other regions such as Central
268 Africa and South America (high BC and OA from open biomass burning). Areas with significant loads
269 can also be seen over global oceans, far from the main emission regions, showing the importance of
270 long-range aerosol transport for both the global and regional climate impact of aerosols.

271 In Table 2, the regional averages of aerosol burdens for the four source regions reveal some
272 differences between the regions. Particularly, for BC and OA, East and South Asia have significantly
273 higher burdens than North America, Europe, Russia/Belarus/Ukraine (henceforth referred to as
274 Russia, for simplicity) and the Middle East. For SO₄, the Middle East ranks among the high-emission
275 source regions. The source regions are also different in terms of meteorology (see Table 2) and surface
276 albedo (not shown), which will influence the local as well as remote effects of emission reductions.
277 For instance, the amount, timing and intensity of precipitation events largely controls the rate of wet
278 removal of fresh aerosols. For year 2010 the average daily precipitation in the Middle East was 0.4
279 mm/day, while in South Asia it was 3.3 mm/day (Table 2). Meanwhile, the South Asian region is also
280 marked by a significantly higher convective mass flux than the other regions, which likely enhances
281 long range transport due to convective lifting of insoluble aerosols to high altitudes. The fractions of
282 BC, OA and SO₄ to the total BC+OA+SO₄ sum are on the other hand quite similar between the
283 regions, with BC contributing 4-8 % of the total, OA contributing 25-45 % of the total, and SO₄
284 contributing 51-70 % of the total (not shown). Europe has a lower fraction of OA and a higher share of
285 SO₄ than the other regions, while the Middle East has a lower BC fraction and higher SO₄ fraction.

286 The relative inter-model standard deviation in emissions is given in the top row of Fig. 2, and
287 demonstrates that for all three species the models disagree the most over the tropics and over the poles.
288 Regionally and annually averaged emissions (second row of Fig. 2) for all three aerosol species are
289 highest in East Asia. The error bars indicate the full range of model results. For BC and SO₄ there is a
290 very limited spread between the models, as all HTAP2 model groups used emission data from the
291 Emissions Database for Global Atmospheric Research (EDGAR) HTAP_v2 emission inventory
292 (Janssens-Maenhout et al., 2015). However, there is a large spread in OA emissions between the
293 models, primarily due to high OA emissions from GEOS5, GEOSCHEMADJOINT and GOCART,
294 but presumably also linked to the above mentioned conversion from OC to OA for some of the
295 models, as well as model differences in the treatment of SOA.

296 In spite of the unified emissions, total aerosol burdens (not shown) vary substantially between the
297 models. This is expected, as there is a broad range of model processes that connect emissions to global
298 aerosol burden, and different models treat these processes differently. For example, the convection
299 schemes used by the different models listed in Table 1 differ markedly. Parametrizations of processes
300 such as wet removal and oxidation will also be sources of inter-model difference, as will their
301 horizontal and vertical resolution. For instance, Molod et al. (2015) performed model simulations of

302 different horizontal resolution with the GEOS5 model, which parameterizes convection using the
303 relaxed Arakawa-Schubert algorithm (RAS). They found that the mass flux decreases with increasing
304 resolution, resulting in reduced low-level drying, which again might increase wet removal and lower
305 the aerosol burden. Kipling et al. (2015) investigated processes important for the shape of vertical
306 aerosol profiles by performing a number of sensitivity tests using the HadGEM3-UKCA model, and
307 comparing the variation in results to the inter-model variation from the AeroCom Phase II control
308 experiment. They found that the vertical profile was controlled mainly by convective transport, in-
309 cloud scavenging and droplet growth by condensation – processes that have widely different
310 parametrizations between models.

311 An HTAP2 model-observation comparison study by Chin et al. (manuscript in preparation) finds that
312 in general, compared to measurements, the two CHASER models typically report too high surface
313 concentrations of SO₄, OA and BC, while OsloCTM3_v02 generally have low values. Figure 3 shows
314 vertically resolved plots of globally averaged mass mixing ratios (MMR) for the three aerosol
315 species, and illustrates that the high values for CHASERT42 and CHASERT106 extend through all
316 vertical layers. It is interesting to note that the CHASER models use a version of the Arakawa-
317 Schubert parametrization of convection, and that the highest-resolution version (T106) has the lowest
318 aerosol burden among the two, which could be related to the findings of Molod et al. (2015) noted
319 above. Note that for SO₄, GOCART and GEOS5 have particularly high MMR aloft, see Fig. 3 (c).

320
321

322 **3.2 Aerosol changes**

323 The third row of Fig. 2 shows the change in global, annual mean aerosol burden following a 20 %
324 emission reduction in the region noted on the x axis. The burden change is clearly highest for the
325 regions with the highest baseline emissions (second row of Fig. 2). The ranges are wider, particularly
326 in the tropical regions, since, as commented above, the processes connecting emissions to burdens
327 vary greatly between the models. The inter-model spread becomes even clearer when expanding the
328 vertical dimension. This is illustrated by Fig. 4, which shows globally averaged vertical profiles of
329 aerosol MMR change per vertical layer for all species, experiments and models. Differences in the
330 vertical profiles, reflecting differences in vertical transport, between the models can be seen.
331 SPRINTARS and the two CHASER models report among the highest MMR changes. For BC,
332 SPRINTARS have particularly large MMR changes for the *RBUreduced* and *MDEreduced*
333 experiments.

334 The *SASreduced* experiment (third row, Fig. 4) is associated with the most pronounced upper-level
335 MMR changes, conceivably because this is the region associated with the highest convective activity.
336 Indeed, the average upward moist convective mass flux in the SAS region is more than double what it
337 is in for instance the NAM region (Table 2). Possibly linked to the treatment of convection in the
338 models, we find that GOCART, GEOSCHEMADJOINT and GEOS5 show particularly high upper-
339 level BC changes from emission perturbations in the SAS region. One common denominator for these
340 two models is the use of the above mentioned RAS algorithm, which in a study based on an earlier
341 version of the GEOS model was found to overestimate convective mass transport (Allen et al., 1997).
342 However, while GEOS5 also has large high-altitude burden changes for both OA and SO₄ for the
343 *SASreduced* experiment, GOCART and GEOSCHEMADJOINT show very weak high-altitude
344 changes compared to the other models in the SO₄ case. Conceivably, wet scavenging, to which SO₄ is
345 more subject than BC, is stronger in GOCART than in other models over this region.

346 Regional increases in aerosol concentrations imposed by emission reductions can be observed for
 347 SPRINTARS and CAMchem, and to a smaller extent also for the CHASER models, GEOS5 and C-
 348 IFS (not shown, but visible in the globally averaged *RBUreduced* and *MDEreduced* plots for OA in
 349 Fig. 4). This occurs mainly for OA and SO₄. Aerosol emission reductions may in these models be
 350 influencing the level of oxidants, which would have feedbacks on the concentrations of OA and SO₄.
 351 A model study by Shindell et al. (2009) demonstrates the importance of aerosol-gas interactions to the
 352 climate impact of mitigations. They point out that the effect on oxidant changes on SO₄ concentrations
 353 are stronger in oxidant-limited regions with high SO₂ emissions, and that greater parts of the
 354 industrialized Northern Hemisphere is, in fact, oxidant limited (Berglen et al., 2004).

355 A contributing cause of the unexpected concentration increases could also be nudging, which is a
 356 simple form of data assimilation that adjusts certain variables of free running climate models to
 357 meteorological re-analysis data – in this case, to constrain the climate to year 2010 meteorology. The
 358 nudging is done differently by the individual model groups. For instance, in SPRINTARS there is no
 359 nudging below altitudes of approximately 300 m, which means that the meteorological field will be
 360 slightly different due to perturbed aerosol effects between the two experiments. This could potentially
 361 involve lower precipitation levels, which would influence the degree of wet removal of particularly
 362 OA and SO₄. Nudging has been shown to have the potential to induce forcings that could change the
 363 base characteristics of a model; Zhang et al. (2014) demonstrated using the CAM5 model that nudging
 364 towards reanalysis data resulted in a substantial reduction in cold clouds. Clearly, perturbation
 365 experiments like the ones analyzed in this paper, performed by models with free-running and nudged
 366 (as opposed to offline) meteorology must be interpreted with caution. A closer investigation of the
 367 cause of the unexpected aerosol concentration increases would be an interesting topic of further
 368 investigations.

369 We have also calculated regional averages of the MMR change profiles for the regions in Fig. 1 (a),
 370 see Fig. 5. The figure shows the rate of MMR change in a receptor region (colored lines) caused by
 371 emission reductions in a source region (rows), for the three aerosol species (columns). These figures
 372 clearly show the effect of long-range aerosol transport on vertical aerosol profiles: notice for instance
 373 the SO₄ burden change profile (rightmost column) for the Arctic (grey), which reaches a maximum at
 374 low altitudes for Russian emission changes (fifth row), but high up for South Asian emission changes
 375 (third row). The HTAP1 study of Shindell et al. (2008) found that upper-troposphere emission-
 376 weighted SO₄ and BC concentrations in the Arctic were greatest for emission changes in South Asia
 377 (in the spring) and East Asia (during other seasons), while low-level emission-weighted changes in
 378 Arctic pollution were dominated by emission changes in Europe. While Fig. 5 does not show
 379 emission-weighted numbers, we see the same tendency of nearby source regions (such as Russia)
 380 causing lower-level changes in the Arctic. The large potential of Russian BC emission to influence
 381 Arctic climate has been pointed out earlier (Sand et al., 2013b; Stohl, 2006).

382

383 3.2.1 Aerosol lifetime

384 Referring to Fig. 2, we have in the bottom row estimated the regional, annually averaged atmospheric
 385 lifetime of the different aerosol species emitted from the six regions, through the relation

$$386 \tau = \Delta BD(Tg) / \Delta Em(Tg \text{ day}^{-1}) \quad (4)$$

387 where ΔEm is the change in emissions on daily timescale within the region (and hence also the global
 388 change), and ΔBD is the resulting change in global aerosol burden. SO₄ has an estimated lifetime of 3-

389 6 days, except for emissions in the MDE region where the model mean lifetime is 11 days, with an
390 inter-model spread from 8 (GOCART) to 17 (CHASERre1) days, corresponding to the models with
391 the lowest and highest SO₄ MMR changes, respectively. OA has slightly higher lifetimes; 5-9 days,
392 except for the MDE regions where the lifetime is above 10 days. This is high compared to the
393 AeroCom model comparison of Tsigaridis et al. (2014), which found a median global OA lifetime of
394 5.4 days (range 3.8–9.6 days). Note that fewer models performed the *MDEreduced* and *RBUreduced*
395 experiments (see Table S-5) and so the estimates for these regions are more uncertain. BC lifetimes are
396 typically around 11 days for emissions in the MDE and SAS regions and 6-8 days in the other regions,
397 which is also higher than the 5 days shown by Samset et al. (2014) to be an upper limit for
398 reproducing remote ocean BC observations. The extended lifetime for aerosols emitted within the SAS
399 region is likely due to more efficient vertical mixing (see Table 2) and low precipitation except during
400 the monsoon season. This finding is consistent with previous studies and the longer lifetime is seen
401 particularly during Northern hemisphere winter (Berntsen et al., 2006). High lifetimes in the MDE
402 region, particularly for OA and SO₄ which are more subject to wet removal, are probably linked to dry
403 atmospheric conditions (see Table 2).

404

405 **3.3 Radiative forcing changes**

406 In Fig. 6 we show annual and regional averages of the AFE profiles used as input to the RF
407 calculations (Samset and Myhre, 2011), for the regions in Fig. 1 (a). Underlying calculations were
408 performed on grid-level using separate profiles for each aerosol species. The global, annual mean BC
409 AFE in Fig. 6 (a) increases strongly with altitude for all regions, rising from about 400 Wg⁻¹ close to
410 the surface to about 3700 Wg⁻¹ at TOA. The reason for this increase is mainly scattering and reflection
411 from underlying clouds, gases and aerosols, the cumulative amount of which increases with altitude.
412 This enhances the amount of short wave radiation that the BC aerosol may absorb, and therefore its
413 radiative impact increases with height. Hence, a given change in BC concentration will have a larger
414 influence on the total TOA forcing if it occurs at high altitudes than if it occurs at lower altitudes. Note
415 that the magnitude as well as the exact shape of the profile varies between the regions, depending on
416 geographic location, climatic factors and surface albedo. For instance, the high surface albedo of the
417 Arctic or the Middle East renders the radiative impact of the dark BC aerosols, and therefore the AFE
418 magnitude, particularly high. Also, the vertical increase in the Middle East is less steep than in the
419 other regions, conceivably due to the lower occurrence of clouds in this area (see Table 2).

420 Figures 6 (b) and 6 (c) show similar curves for OA and SO₄ respectively, with a weaker dependency
421 on altitude compared to BC. For SO₄, a strong maximum close to 900hPa can be seen, mainly related
422 to humidity and hygroscopic growth (Samset and Myhre, 2011) which significantly enhances the
423 scattering properties of SO₄ aerosols (Haywood et al., 1997; Myhre et al., 2004; Bian et al., 2009), but
424 which is less relevant for OA. This is well illustrated by looking at the regionally averaged relative
425 humidity from MERRA data in Fig. 7, which shows that the Middle East, which has a weak relative
426 humidity (RH) profile (as well as low average cloud cover; Table 2), is the region with the weakest
427 SO₄ AFE profile. Meanwhile, remote ocean regions typically associated with persistent low-level
428 clouds (e.g. the South Atlantic or the North/South Pacific) are the areas with the most pronounced SO₄
429 AFE profiles (not shown).

430 Combining these AFE profiles with aerosol burden changes for each grid cell, month and vertical level
431 (see Eq. (1)), we obtain direct radiative forcing. Table 3 shows the global mean direct RF, per Tg
432 emission change, for the three species and six experiments. The forcing ranges between 51.9 and
433 210.8 mWm⁻² Tg⁻¹ for BC, between -2.4 and -17.9 mWm⁻² Tg⁻¹ for OA, and between -3.6 and -10.3

434 $\text{Wm}^{-2} \text{Tg}^{-1}$ for SO_4 . The HTAP1 study by Yu et al. (2013), which is based on data from nine CTMs and
435 uses emissions for year 2001 as a baseline, obtained for instance an RF of $27.3 \text{ mWm}^{-2} \text{Tg}^{-1}$ for BC
436 from emission reductions in the NAM region. This is substantially lower than our $51.9 \text{ mWm}^{-2} \text{Tg}^{-1}$ for
437 the same case, which is related to the host model used to calculate the AFE: As mentioned in Sect.
438 2.2., we calculate RF based on the OsloCTM2 model, which ranks among the models with highest
439 AFE for BC in an AeroCom intercomparison study (Myhre et al., 2013). Conversely, GOCART,
440 which was used to calculate the RF in Yu et al. (2013), had the lowest AFE for BC among the
441 investigated AeroCom models. The same AeroCom study found that AFE for SO_4 was much more
442 similar between these two host models, and while we find for NAM an SO_4 RF of $-4.5 \text{ mWm}^{-2} \text{Tg}^{-1}$,
443 the number from Yu et al. (2013) is a fairly similar $-3.9 \text{ mWm}^{-2} \text{Tg}^{-1}$. See Samset and Myhre (2015)
444 for a discussion of the AFE in OsloCTM2.

445 Mitigations in the Middle East give the largest forcing per Tg emission change for all aerosol species.
446 The particularly large BC forcing ($201.8 \text{ mWm}^{-2} \text{Tg}^{-1}$) is probably related to the region's high surface
447 albedo, as also found in Samset and Myhre (2015). For OA and SO_4 , which are more subject to wet
448 scavenging, the dry atmospheric conditions of the region (Table 2) favor long lifetimes, as shown in
449 Fig. 2 (bottom row). The opposite can be seen in Russia, for which OA and SO_4 forcing is the
450 weakest; here, the lifetime is the shortest among the regions for these species, and the AFE values are
451 the smallest (solid blue lines, Fig. 6). Note that while the annually averaged precipitation amount for
452 2010 was not particularly high in RBU, the region has a high average cloud cover (Table 2 and Fig. 7),
453 which contributes to wet scavenging. The SAS region also has high RF for all three aerosol species.
454 For BC, this may be related to the region's high convective activity, which promotes long-range
455 aerosol transport and therefore high-altitude MMR changes, which due to the BC AFE profile
456 increases the resulting forcing. A particularly intensive monsoon associated with the strong La Niña
457 event in 2010 may have contributed to higher convective lifting (and associated effects on the RF) in
458 this analyses compared to e.g. Yu et al. (2013) or Shindell et al. (2008).

459 In parentheses in Table 3, we show the relative standard deviation (RSD) values for the RF
460 calculations – i.e. the sample standard deviation divided by the mean – as a representation of inter-
461 model spread. In Yu et al. (2013) inter-model differences were also found to be substantial, and one
462 might expect the spread to be larger due to the large variation in emissions used by the HTAP1
463 models. However, comparing RSD of emission-weighted RF from Yu et al. (2013) HTAP1 data
464 (based on their Table 6) to the present HTAP2 data (Table 3), there is no clear tendency that the inter-
465 model spread for HTAP2 is smaller. In fact, while the RSD for emission-weighted RF for BC
466 averaged over the four common source regions (NAM, EUR, SAS and EAS) was higher for HTAP1
467 (0.60) than for HTAP2 (0.37), the opposite was true for the SO_4 forcing (RSD of 0.23 and 0.43 for
468 HTAP1 and HTAP2, respectively). The mixture of models (only CTMs in HTAP1 and both CTMs
469 and GCMs in HTAP2), the different meteorological years used (2001 in HTAP1 and 2010 in HTAP2),
470 as well as the fact that HTAP1 region definitions comprised larger areas with much ocean, are
471 contributing causes that direct comparison of inter-model spread between the two analyses is difficult.
472 In either case, however, the large ranges in AFE values demonstrates that differences between aerosol
473 optical properties, treatment of transport and wet removal, and model native meteorology are still
474 large. Our results, which are based on simulations using the same set of emissions, also shows notable
475 inter-model differences. This underlines the importance of model variations in the various aerosol-
476 related parametrizations – in agreement with previous studies (Kasoar et al., 2016; Textor et al., 2007;
477 Wilcox et al., 2015).

478 A more detailed perspective of the global forcing averages of Table 3 can be found in Fig. 8, which
479 shows the RF, at top-of-atmosphere, estimated to be exerted due to the aerosol abundance change in

480 each OsloCTM2 model layer. The diversity between models seen in the MMR change in Fig. 4 is
481 naturally still present, but, in particular for BC, the relative importance of low and high altitudes has
482 shifted. The strongly increasing BC AFE with altitude dampens BC variability close to the surface,
483 and emphasizes differences at high altitude. For SO₄, the peak in AFE close to 900hPa coincides with
484 regions of high concentration, leading to increased effective variability in RF exerted close to the
485 surface. For the same reasons, the particularly large upper-level MMR differences between the models
486 for the *SASreduced* experiment (Fig. 4) show enhanced RF for BC but dampened for SO₄.

487

488 **3.4 Local versus remote impacts of emission mitigation**

489 We move on to quantify how emission mitigations in the six source regions influence radiative forcing
490 both locally within the source region and in other receptor regions. The leftmost column of Fig. 9
491 shows the effect of domestic emission reductions on local RF from SO₄, OA and BC (Fig. 9 (a), 9 (c)
492 and 9 (e), respectively). To account for the effect of the large variation in baseline emissions between
493 the source regions, we have divided the RF by the annually averaged multi-model median emission
494 change of the source region in question (this gives the forcing efficiency for a given emission change,
495 but to avoid confusion with the aerosol forcing efficiency, or AFE, profiles used to calculate the RF
496 we will refer to this quantity as the emission-weighted forcing). Hence, while e.g. EAS has much
497 larger SO₂ emissions than the other regions (Fig. 2) and therefore much larger absolute local forcing
498 (not shown), the regional difference in the emission-weighted forcing in Fig. 9a is caused by other
499 factors than the difference in emission levels. For all species, however, the emission-weighted
500 domestic forcings for the SAS and MDE regions stand out as substantially higher than the other
501 regions. The numerical values corresponding to Fig. 9 are presented in Tables S-6 through S-8.

502 Notice that Fig. 9 (a), 9 (c) and 9 (e) have two bars per source region – one solid and one dashed. The
503 solid bar shows the emission-weighted forcing calculated by Eq. (1), fully accounting for the vertical
504 aerosol and AFE profile. The hatched bar, however, shows a version calculated by Eq. (2), where we
505 instead use vertically averaged AFE numbers and total column burden changes (equivalent to the
506 method that was used for HTAP1 results in Yu et al. (2013)). We can thus study how accounting for
507 the vertical profiles influences the magnitude of the emission-weighted forcing. For SO₄, the vertically
508 resolved RF calculation gives stronger emission-weighted forcings than the ones using column
509 burdens: averaged across the regions, treating vertical profiles strengthens SO₄ emission-weighted RF
510 by 25 %. The reason for this is that domestic emission reductions cause changes in atmospheric
511 aerosol concentrations primarily at low levels, where AFE for SO₄ is high. For BC, on the other hand,
512 RF is reduced by 37 % when accounting for the vertical dimension, because AFE for BC is weak in
513 the lower atmosphere. For OA, including the vertical information induces only a small increase in
514 emission-weighted RF of about 8 %. This is unsurprising, given the weak altitude dependence of OA
515 AFE as shown in Fig. 6.

516 The rightmost column of Fig. 9 – Fig. 9 (b), 9 (d) and 9 (f) – shows how emission reductions in
517 different source regions (see x axis) influence the emission-weighted forcing in other receptor regions
518 (indicated by the colors of the bars clustered above each source region). In general, the extra-regional
519 forcing is largest for nearby upwind source regions. For instance, for all aerosol species perturbations
520 in North America have a large effect on the emission-weighted forcing in Europe. Russia, closely
521 followed by Europe, is the region with the largest influence on the Arctic, and Russia and Europe also
522 have a strong influence on each other. We similarly find that South Asia has a very large impact on the
523 emission-weighted forcing in East Asia. However, as noted by Chakraborty et al. (2015) who studied
524 ozone transport between South and East Asia based on HTAP1 simulations, the influence on South

525 Asia on East Asia is limited by the onset of the monsoon season, during which the prevailing wind
526 pattern turns the influence the other way around. In fact, Chakraborty et al. (2015) found that when
527 focusing on the populated parts of these regions, the emission changes over East Asia had a larger
528 impact on populated parts of South Asia than vice versa, due to the specific monthly variations of the
529 meteorological conditions. Another HTAP1 study investigating reductions in methane and ozone
530 precursor emissions found that among the four source regions NAM, EUR, SAS and EAS, the SAS
531 region posed the largest emission-weighted influence in terms of radiative forcing, as this region was
532 located closest to the equator and therefore had the strongest photochemistry, but also due to the
533 strong vertical mixing during the monsoon season (Fry et al., 2012).

534 While it is useful to compare extra-regional effects per Tg emission reduction, the potential for sizable
535 emission reductions is likely to be lower in the regions with the lowest baseline emissions (Table 2).
536 When we estimated the impact of intercontinental transport by calculating the RERER coefficient (Eq.
537 3), we therefore use absolute (as opposed to emission-weighted) numbers. Table 4 shows RERER
538 values for all species and regions. For burden change (top half of Table 4), SO₄ RERER is found to be
539 between 0.32 and 0.76 for the various regions, with high values indicating that a region is strongly
540 influenced by long-range transport from other regions. OA burden RERER ranges from 0.09 to 0.90,
541 while BC burden RERER ranges from 0.18 to 0.87. The RERER values are consistent with Chin et al.
542 (manuscript in preparation), who investigated RERER for HTAP2 data based on surface
543 concentrations. Due to the experiment design, the source regions are not fully identical between
544 HTAP1 and HTAP2, so for easier comparison to HTAP1 studies, a version of Table 4 calculated using
545 the HTAP1 definitions for receptor regions is included in Table S-9. The main features are the same as
546 in Table 4, but the values are in general higher, as expected since the receptor regions are larger for
547 HTAP1 than for HTAP2. This difference is most prominent for Europe.

548 To investigate the impact of the vertical distribution of aerosols, we also calculate RERER for RF
549 estimated with the vertically resolved AFE distributions (see bottom half of Table 4.) RERER for SO₄
550 and OA are broadly similar for burden change and RF. BC RERER, however, is markedly higher (by
551 30 %, averaged over all source regions) for RF. This is due to long range transport predominantly
552 taking place at high altitudes, where BC AFE is strong. Hence any transported BC will have a higher
553 impact on the RF in remote regions, relative to the source region where it originates close to the
554 ground. For OA and BC, the RERER for the SAS region is the lowest among the regions, which
555 means that the region to a lesser extent is influenced by other regions. The RBU and MDE regions
556 stand out with very high RERER values, indicating that the regions are very sensitive to extra-regional
557 emission changes. For BC, a high sensitivity of the NAM region to extra-regional emissions is
558 witnessed by a high RERER value. This sensitivity of North America to emission changes in other
559 regions has also been noted in other studies, e.g. in a satellite study by Yu et al. (2012).

560 To visualize the impact of intercontinental transport on the RF that a given receptor region experiences
561 due to emission reductions in different source regions, we present in Figure 10 a stacked bar plot. For
562 each species and averaged over the different receptor regions (see x axis), the colors show how much a
563 20% emission reduction in each of the source region contributes to the summed forcing from all
564 source regions, in percent. The summed forcing that a receptor region experiences from the six
565 experiments is given above each bar. Note that as the individual source regions' contribution is
566 calculated relative to the summed contribution of the six source regions and not relative to a global
567 emission reduction, as in the calculation of RERER, the numbers in Tab. 4 will be qualitatively but not
568 quantitatively comparable to this figure. Figure 10 illustrates for instance that the main contributor to
569 the high RERER value in the NAM region is EAS: for BC, more than 40 % of the summed forcing
570 originates from emission changes in EAS. The HTAP1 study by Yu et al. (2013) also concluded that

571 East Asia posed the largest influence on North America for BC RF. However, they also found that for
572 SO₄ RF, South Asia was strongly influenced by emission changes in Europe. This we do not see in our
573 results, probably because the baseline emissions in Yu et al. (2013) were for year 2001, for which
574 European SO₄ emissions were substantially higher and Indian emissions lower. Other HTAP1 studies
575 also point to a strong influence of European emission changes: Anenberg et al. (2014) studied impacts
576 of intercontinental transport of fine particulate matter on human mortality, and found that 17 and 13 %
577 of premature deaths caused by inhalation of fine particulate matter could be avoided by reducing North
578 American and European emissions, as opposed to 4 and 2 % for South and East Asia. The main reason
579 for this, however, was higher downwind populations for the two first regions as opposed to the two
580 last. Figure 10 shows that domestic mitigations dominate the contribution to the total RF in South and
581 East Asia, and these are also the regions with the largest forcing contributions to other regions.
582 However, it is important to note that this relationship is strongly driven by the fact that the baseline
583 emissions (and hence the 20% emission changes) in EAS and SAS are the largest of all regions, and as
584 we saw from Fig. 9, the relationship changes when looking at emission-weighted numbers: While Fig.
585 10 shows e.g. a strong contribution from EAS to the forcing in RBU, Fig. 9 demonstrated that per Tg
586 emission reduction EUR has a much stronger influence on RBU than EAS.

587

588 **4. Summary and Conclusions**

589 We have compared RF for the direct aerosol effect from regional 20 % reductions in anthropogenic
590 aerosol emissions, for ten global climate and chemical transport models participating in the HTAP2
591 multi-model exercise for the year 2010. We focused on the model experiments simulating emission
592 reductions in North America, Europe, South Asia, East Asia, Russia/Belarus/Ukraine and the
593 Middle East. We find that the globally averaged TOA radiative forcing exerted per Tg of emission
594 reduction varies between the source regions from 51.9 to 210.8 mWm⁻² Tg⁻¹ for BC, from -2.4 to -17.9
595 mWm⁻² Tg⁻¹ for OA, and from -3.6 to -10.3 Wm⁻² Tg⁻¹ for SO₄. For all species, the globally averaged
596 emission-weighted forcing from the Middle East was larger than from emission reductions in the other
597 regions, primarily due to the long lifetime of aerosols originating from this region. For BC, the
598 emission-weighted forcing was particularly strong due to the high surface albedo of the Middle East.
599 The second highest values were caused by emission changes in South Asia, due to the high convective
600 activity, relatively long aerosol lifetime and the low-latitude location. This region, as well as the East
601 Asian region, also induced the largest regionally averaged emission-weighted forcing in a number of
602 investigated receptor regions, especially for BC. Mitigations in Europe have strongest impacts on
603 Russia, the Arctic and the Middle East. Note that relatively long aerosol lifetimes are simulated in this
604 study, and the BC lifetime is longer than found in models reproducing the vertical profile during the
605 HIPPO campaigns in the Pacific Ocean (Samset et al., 2014). A shorter lifetime of BC reduces the RF
606 of the direct aerosol effect substantially (Hodnebrog et al., 2014).

607

608 Although extra-regional mitigations have important contributions to the RF of a given region, the local
609 influence of emission reductions is for most regions the dominant one. There are however, exceptions:
610 BC emissions in East Asia are found to be more important to North America than domestic mitigation,
611 which is consistent with previous findings pertaining the 2000s. A similar feature was found for
612 Russia for OA and BC; the RF contribution from mitigations in Europe and East Asia outweighs the
613 region's own influence – at least when mitigations are defined as 20% of the region's baseline
614 emissions. For the Middle East, OA and BC forcing is dominated by influence from East Asia.

615 We have also gone beyond previous HTAP studies and investigate the impact of using vertically
616 resolved concentrations of atmospheric aerosols combined with vertically resolved AFE distributions
617 when estimating global mean aerosol radiative forcing and intercontinental transport. We find that this
618 strengthens SO₄ RF for all regions, relative to using vertically averaged distributions. BC RF weakens
619 when using fully resolved distributions, due to a larger weight being put on BC near sources, close to
620 the ground, where BC AFE is lower. The same feature, only weaker due to a weaker AFE profile, can
621 be observed for OA. While atmospheric transport of SO₄ and OA is only weakly affected, the
622 influence of inter-continental transport to BC forcing is strengthened by 30 % when accounting for the
623 vertical aspect, because long-range transport leads primarily to aerosol changes at high altitudes,
624 where BC AFE is strong.

625
626
627

628 **Acknowledgement:** This work was supported by the Research Council of Norway through the grants
629 AC/BC (240372), NetBC (244141) and SLAC. The CESM project is supported by the National
630 Science Foundation and the Office of Science (BER) of the U. S. Department of Energy. The National
631 Center for Atmospheric Research is funded by the National Science Foundation. The SPRINTARS is
632 supported by the supercomputer system of the National Institute for Environmental Studies, Japan, the
633 Environment Research and Technology Development Fund (S-12-3) of the Ministry of the
634 Environment, Japan, and JSPS KAKENHI grants 15H01728 and 15K12190. Johannes Flemming's
635 contribution has been supported by the Copernicus Atmosphere Service. This study also benefitted
636 from the Norwegian research council projects #235548 (Role of SLCF in Global Climate Regime) and
637 #229796 (AeroCom-P3).

638 **References**

- 639 Allen, D. J., Pickering, K. E., and Molod, A.: An evaluation of deep convective mixing in the Goddard
640 Chemical Transport Model using International Satellite Cloud Climatology Project cloud parameters,
641 *Journal of Geophysical Research: Atmospheres*, 102, 25467-25476, 10.1029/97JD02401, 1997.
- 642 Anenberg, S. C., West, J. J., Yu, H., Chin, M., Schulz, M., Bergmann, D., Bey, I., Bian, H., Diehl, T., Fiore,
643 A., Hess, P., Marmer, E., Montanaro, V., Park, R., Shindell, D., Takemura, T., and Dentener, F.: Impacts
644 of intercontinental transport of anthropogenic fine particulate matter on human mortality, *Air
645 Quality, Atmosphere & Health*, 7, 369-379, 10.1007/s11869-014-0248-9, 2014.
- 646 Ban-Weiss, G. A., Cao, L., Bala, G., and Caldeira, K.: Dependence of climate forcing and response on
647 the altitude of black carbon aerosols, *Climate Dynamics*, 38, 897-911, 10.1007/s00382-011-1052-y,
648 2012.
- 649 Berglen, T. F., Berntsen, T. K., Isaksen, I. S. A., and Sundet, J. K.: A global model of the coupled
650 sulfur/oxidant chemistry in the troposphere: The sulfur cycle, *Journal of Geophysical Research:*
651 *Atmospheres*, 109, n/a-n/a, 10.1029/2003JD003948, 2004.
- 652 Berntsen, T., Fuglestad, J., Myhre, G., Stordal, F., and Berglen, T. F.: Abatement of greenhouse
653 gases: Does location matter?, *Climatic Change*, 74, 377-411, 2006.
- 654 Bian, H., Chin, M., Rodriguez, J. M., Yu, H., Penner, J. E., and Strahan, S.: Sensitivity of aerosol optical
655 thickness and aerosol direct radiative effect to relative humidity, *Atmos Chem Phys*, 9, 2375-2386,
656 2009.
- 657 Bollasina, M. A., Ming, Y., and Ramaswamy, V.: Anthropogenic Aerosols and the Weakening of the
658 South Asian Summer Monsoon, *Science*, 334, 502-505, 10.1126/science.1204994, 2011.
- 659 Bond, T. C., and Bergstrom, R. W.: Light Absorption by Carbonaceous Particles: An Investigative
660 Review, *Aerosol Science and Technology*, 40, 27-67, 10.1080/02786820500421521, 2006.
- 661 Boucher, O., Randall, D., Artaxo, P., Bretherton, C., Feingold, G., Forster, P., Kerminen, V.-M., Kondo,
662 Y., Liao, H., Lohmann, U., Rasch, P., Satheesh, S. K., Sherwood, S., Stevens, B., and Zhang, X. Y.: Clouds
663 and Aerosols. In: *Climate Change 2013: The Physical Science Basis. Contribution of Working Group I
664 to the Fifth Assessment Report of the Intergovernmental Panel on Climate Change* [Stocker, T.F., D.
665 Qin, G.-K. Plattner, M. Tignor, S.K. Allen, J. Boschung, A. Nauels, Y. Xia, V. Bex and P.M. Midgley
666 (eds.)], Cambridge University Press, Cambridge, United Kingdom and New York, NY, USA., 2013.
- 667 Brauer, M., Freedman, G., Frostad, J., van Donkelaar, A., Martin, R. V., Dentener, F., Dingenen, R. v.,
668 Estep, K., Amini, H., Apte, J. S., Balakrishnan, K., Barregard, L., Broday, D., Feigin, V., Ghosh, S., Hopke,
669 P. K., Knibbs, L. D., Kokubo, Y., Liu, Y., Ma, S., Morawska, L., Sangrador, J. L. T., Shaddick, G.,
670 Anderson, H. R., Vos, T., Forouzanfar, M. H., Burnett, R. T., and Cohen, A.: Ambient Air Pollution
671 Exposure Estimation for the Global Burden of Disease 2013, *Environmental Science & Technology*, 50,
672 79-88, 10.1021/acs.est.5b03709, 2016.
- 673 Chakraborty, T., Beig, G., Dentener, F. J., and Wild, O.: Atmospheric transport of ozone between
674 Southern and Eastern Asia, *Science of The Total Environment*, 523, 28-39,
675 <http://dx.doi.org/10.1016/j.scitotenv.2015.03.066>, 2015.
- 676 Chikira, M., and Sugiyama, M.: A Cumulus Parameterization with State-Dependent Entrainment Rate.
677 Part I: Description and Sensitivity to Temperature and Humidity Profiles, *Journal of the Atmospheric
678 Sciences*, 67, 2171-2193, 10.1175/2010JAS3316.1, 2010.

679 Chin, M., Rood, R. B., Lin, S.-J., Müller, J.-F., and Thompson, A. M.: Atmospheric sulfur cycle simulated
680 in the global model GOCART: Model description and global properties, *Journal of Geophysical*
681 *Research: Atmospheres*, 105, 24671-24687, 10.1029/2000JD900384, 2000.

682 Colarco, P., da Silva, A., Chin, M., and Diehl, T.: Online simulations of global aerosol distributions in
683 the NASA GEOS-4 model and comparisons to satellite and ground-based aerosol optical depth,
684 *Journal of Geophysical Research: Atmospheres*, 115, n/a-n/a, 10.1029/2009JD012820, 2010.

685 Fierz-Schmidhauser, R., Zieger, P., Wehrle, G., Jefferson, A., Ogren, J. A., Baltensperger, U., and
686 Weingartner, E.: Measurement of relative humidity dependent light scattering of aerosols, *Atmos.*
687 *Meas. Tech.*, 3, 39-50, 10.5194/amt-3-39-2010, 2010.

688 Fitzgerald, J. W.: Approximation Formulas for the Equilibrium Size of an Aerosol Particle as a Function
689 of Its Dry Size and Composition and the Ambient Relative Humidity, *Journal of Applied Meteorology*,
690 14, 1044-1049, doi:10.1175/1520-0450(1975)014<1044:AFFTES>2.0.CO;2, 1975.

691 Flemming, J., Huijnen, V., Arteta, J., Bechtold, P., Beljaars, A., Blechschmidt, A. M., Diamantakis, M.,
692 Engelen, R. J., Gaudel, A., Inness, A., Jones, L., Josse, B., Katragkou, E., Marecal, V., Peuch, V. H.,
693 Richter, A., Schultz, M. G., Stein, O., and Tsikerdekis, A.: Tropospheric chemistry in the Integrated
694 Forecasting System of ECMWF, *Geosci. Model Dev.*, 8, 975-1003, 10.5194/gmd-8-975-2015, 2015.

695 Fry, M. M., Naik, V., West, J. J., Schwarzkopf, M. D., Fiore, A. M., Collins, W. J., Dentener, F. J.,
696 Shindell, D. T., Atherton, C., Bergmann, D., Duncan, B. N., Hess, P., MacKenzie, I. A., Marmer, E.,
697 Schultz, M. G., Szopa, S., Wild, O., and Zeng, G.: The influence of ozone precursor emissions from four
698 world regions on tropospheric composition and radiative climate forcing, *Journal of Geophysical*
699 *Research: Atmospheres*, 117, n/a-n/a, 10.1029/2011JD017134, 2012.

700 Galmarini, S. K., B., Solazzo, E.; Keating, T.; Hogrefe, C.; Schulz, M.; Griesfeller, J.; Janssens-Maenhout,
701 G.; Carmichael, G.; Fu, J.; Denterner, F.: Harmonization of the multi-scale multi-model activities
702 HTAP, AQMEII and MICS-Asia: simulations, emission inventories, boundary conditions and output
703 formats, To be submitted to *Atmos. Chem. Phys.*, 2016.

704 Geng, F. H., Hua, J., Mu, Z., Peng, L., Xu, X. H., Chen, R. J., and Kan, H. D.: Differentiating the
705 associations of black carbon and fine particle with daily mortality in a Chinese city, *Environ Res*, 120,
706 27-32, 2013.

707 Goswami, B. N., and Xavier, P. K.: ENSO control on the south Asian monsoon through the length of
708 the rainy season, *Geophysical Research Letters*, 32, n/a-n/a, 10.1029/2005GL023216, 2005.

709 Hack, J. J., Caron, J. M., Yeager, S. G., Oleson, K. W., Holland, M. M., Truesdale, J. E., and Rasch, P. J.:
710 Simulation of the Global Hydrological Cycle in the CCSM Community Atmosphere Model Version 3
711 (CAM3): Mean Features, *Journal of Climate*, 19, 2199-2221, 10.1175/JCLI3755.1, 2006.

712 Haywood, J. M., Ramaswamy, V., and Donner, L. J.: A limited-area-model case study of the effects of
713 sub-grid scale Variations in relative humidity and cloud upon the direct radiative forcing of sulfate
714 aerosol, *Geophys Res Lett*, 24, 143-146, 10.1029/96gl03812, 1997.

715 Haywood, J. M., and Shine, K. P.: Multi-spectral calculations of the direct radiative forcing of
716 tropospheric sulphate and soot aerosols using a column model, *Quarterly Journal of the Royal*
717 *Meteorological Society*, 123, 1907-1930, 10.1002/qj.49712354307, 1997.

718 Henze, D. K., Hakami, A., and Seinfeld, J. H.: Development of the adjoint of GEOS-Chem, *Atmos.*
719 *Chem. Phys.*, 7, 2413-2433, 10.5194/acp-7-2413-2007, 2007.

720 Hodnebrog, Ø., Myhre, G., and Samset, B. H.: How shorter black carbon lifetime alters its climate
721 effect, *Nat Commun*, 5, 10.1038/ncomms6065, 2014.

722 HTAP: Hemispheric Transport of Air Pollution, Part A: Ozone and particulate matter, Geneva,
723 Switzerland, 2010.

724 Huang, J., Minnis, P., Chen, B., Huang, Z., Liu, Z., Zhao, Q., Yi, Y., and Ayers, J. K.: Long-range transport
725 and vertical structure of Asian dust from CALIPSO and surface measurements during PACDEX, *Journal*
726 *of Geophysical Research: Atmospheres*, 113, n/a-n/a, 10.1029/2008JD010620, 2008.

727 Janssen, N. A. H. e. a.: Health Effects of Black Carbon World Health Organization, 2012.

728 Janssens-Maenhout, G., Crippa, M., Guizzardi, D., Dentener, F., Muntean, M., Pouliot, G., Keating, T.,
729 Zhang, Q., Kurokawa, J., Wankmüller, R., Denier van der Gon, H., Kuenen, J. J. P., Klimont, Z., Frost,
730 G., Darras, S., Koffi, B., and Li, M.: HTAP_v2.2: a mosaic of regional and global emission grid maps for
731 2008 and 2010 to study hemispheric transport of air pollution, *Atmos. Chem. Phys.*, 15, 11411-11432,
732 10.5194/acp-15-11411-2015, 2015.

733 Kasoar, M., Voulgarakis, A., Lamarque, J. F., Shindell, D. T., Bellouin, N., Collins, W. J., Faluvegi, G.,
734 and Tsigaridis, K.: Regional and global temperature response to anthropogenic SO₂ emissions from
735 China in three climate models, *Atmos. Chem. Phys.*, 16, 9785-9804, 10.5194/acp-16-9785-2016,
736 2016.

737 Khain, A. P.: Notes on state-of-the-art investigations of aerosol effects on precipitation: a critical
738 review, *Environmental Research Letters*, 4, 015004, 2009.

739 Kipling, Z., Stier, P., Johnson, C. E., Mann, G. W., Bellouin, N., Bauer, S. E., Bergman, T., Chin, M.,
740 Diehl, T., Ghan, S. J., Iversen, T., Kirkevåg, A., Kokkola, H., Liu, X., Luo, G., van Noije, T., Pringle, K. J.,
741 von Salzen, K., Schulz, M., Seland, Ø., Skeie, R. B., Takemura, T., Tsigaridis, K., and Zhang, K.: What
742 controls the vertical distribution of aerosol? Relationships between process sensitivity in HadGEM3–
743 UKCA and inter-model variation from AeroCom Phase II, *Atmos. Chem. Phys. Discuss.*, 15, 25933–
744 25980, 10.5194/acpd-15-25933-2015, 2015.

745 Koch, D., and Del Genio, A. D.: Black carbon semi-direct effects on cloud cover: review and synthesis,
746 *Atmos. Chem. Phys.*, 10, 7685-7696, 10.5194/acp-10-7685-2010, 2010.

747 Liu, B., Xu, M., and Henderson, M.: Where have all the showers gone? Regional declines in light
748 precipitation events in China, 1960–2000, *International Journal of Climatology*, 31, 1177-1191,
749 10.1002/joc.2144, 2011.

750 Liu, D., Wang, Z., Liu, Z., Winker, D., and Trepte, C.: A height resolved global view of dust aerosols
751 from the first year CALIPSO lidar measurements, *Journal of Geophysical Research: Atmospheres*, 113,
752 n/a-n/a, 10.1029/2007JD009776, 2008.

753 Lohmann, U., and Feichter, J.: Global indirect aerosol effects: a review, *Atmos. Chem. Phys.*, 5, 715–
754 737, 10.5194/acp-5-715-2005, 2005.

755 Ming, Y., Ramaswamy, V., and Persad, G.: Two opposing effects of absorbing aerosols on global-mean
756 precipitation, *Geophysical Research Letters*, 37, n/a-n/a, 10.1029/2010GL042895, 2010.

757 Molod, A., Takacs, L., Suarez, M., and Bacmeister, J.: Development of the GEOS-5 atmospheric
758 general circulation model: evolution from MERRA to MERRA2, *Geosci. Model Dev.*, 8, 1339-1356,
759 10.5194/gmd-8-1339-2015, 2015.

760 Moorthi, S., and Suarez, M. J.: Relaxed Arakawa-Schubert. A Parameterization of Moist Convection
761 for General Circulation Models, *Monthly Weather Review*, 120, 978-1002, 10.1175/1520-
762 0493(1992)120<0978:RASAP0>2.0.CO;2, 1992.

763 Myhre, G., Stordal, F., Berglen, T., Sundet, J. K., and Isaksen, I. S. A.: Uncertainties in the Radiative
764 Forcing Due to Sulfate Aerosols, *Journal of the Atmospheric Sciences*, 2004.

765 Myhre, G., Bellouin, N., Berglen, T. F., Berntsen, T. K., Boucher, O., Grini, A. L. F., Isaksen, I. S. A.,
766 Johnsrud, M., Mishchenko, M. I., Stordal, F., and Tanré, D.: Comparison of the radiative properties
767 and direct radiative effect of aerosols from a global aerosol model and remote sensing data over
768 ocean, *Tellus B*, 59, 115-129, 10.1111/j.1600-0889.2006.00226.x, 2007.

769 Myhre, G., Berglen, T. F., Johnsrud, M., Hoyle, C. R., Berntsen, T. K., Christopher, S. A., Fahey, D. W.,
770 Isaksen, I. S. A., Jones, T. A., Kahn, R. A., Loeb, N., Quinn, P., Remer, L., Schwarz, J. P., and Yttri, K. E.:
771 Modelled radiative forcing of the direct aerosol effect with multi-observation evaluation, *Atmos.*
772 *Chem. Phys.*, 9, 1365-1392, 10.5194/acp-9-1365-2009, 2009.

773 Myhre, G., Samset, B. H., Schulz, M., Balkanski, Y., Bauer, S., Berntsen, T. K., Bian, H., Bellouin, N.,
774 Chin, M., Diehl, T., Easter, R. C., Feichter, J., Ghan, S. J., Hauglustaine, D., Iversen, T., Kinne, S.,
775 Kirkevåg, A., Lamarque, J. F., Lin, G., Liu, X., Lund, M. T., Luo, G., Ma, X., van Noije, T., Penner, J. E.,
776 Rasch, P. J., Ruiz, A., Seland, Ø., Skeie, R. B., Stier, P., Takemura, T., Tsigaridis, K., Wang, P., Wang, Z.,
777 Xu, L., Yu, H., Yu, F., Yoon, J. H., Zhang, K., Zhang, H., and Zhou, C.: Radiative forcing of the direct
778 aerosol effect from AeroCom Phase II simulations, *Atmos. Chem. Phys.*, 13, 1853-1877, 10.5194/acp-
779 13-1853-2013, 2013.

780 Myhre, G., and Samset, B. H.: Standard climate models radiation codes underestimate black carbon
781 radiative forcing, *Atmos. Chem. Phys.*, 15, 2883-2888, 10.5194/acp-15-2883-2015, 2015.

782 Rienecker, M. M., Suarez, M. J., Todling, R., Bacmeister, J., Takacs, L., Liu, H.-C., Gu, W., Sienkiewicz,
783 M., Koster, R. D., Gelaro, R., Stajner, I., and Nielsen, J. E.: The GEOS-5 Data Assimilation System —
784 Documentation of Versions 5.0.1, 5.1.0, and 5.2.0, NASA, 2008.

785 Samset, and Myhre: Climate response to externally mixed black carbon as a function of altitude,
786 *Journal of Geophysical Research: Atmospheres*, 120, 2014JD022849, 10.1002/2014JD022849, 2015.

787 Samset, B. H., and Myhre, G.: Vertical dependence of black carbon, sulphate and biomass burning
788 aerosol radiative forcing, *Geophysical Research Letters*, 38, n/a-n/a, 10.1029/2011GL049697, 2011.

789 Samset, B. H., Myhre, G., Schulz, M., Balkanski, Y., Bauer, S., Berntsen, T., Bian, H., Bellouin, N., Diehl,
790 T., Easter, R. C., Ghan, S. J., Iversen, T., Kinne, S., Kirkevåg, A., Lamarque, J. F., Lin, G., Liu, X., Penner,
791 J. E., Seland, Ø., Skeie, R. B., Stier, P., Takemura, T., Tsigaridis, K., and Zhang, K.: Black carbon vertical
792 profiles strongly affect its radiative forcing uncertainty, *Atmos. Chem. Phys.*, 13, 2423-2434,
793 10.5194/acp-13-2423-2013, 2013.

794 Samset, B. H., Myhre, G., Herber, A., Kondo, Y., Li, S. M., Moteki, N., Koike, M., Oshima, N., Schwarz,
795 J. P., Balkanski, Y., Bauer, S. E., Bellouin, N., Berntsen, T. K., Bian, H., Chin, M., Diehl, T., Easter, R. C.,
796 Ghan, S. J., Iversen, T., Kirkevåg, A., Lamarque, J. F., Lin, G., Liu, X., Penner, J. E., Schulz, M., Seland,
797 Ø., Skeie, R. B., Stier, P., Takemura, T., Tsigaridis, K., and Zhang, K.: Modelled black carbon radiative
798 forcing and atmospheric lifetime in AeroCom Phase II constrained by aircraft observations, *Atmos.*
799 *Chem. Phys.*, 14, 12465-12477, 10.5194/acp-14-12465-2014, 2014.

800 Sand, M., Berntsen, T. K., Kay, J. E., Lamarque, J. F., Seland, Ø., and Kirkevåg, A.: The Arctic response
801 to remote and local forcing of black carbon, *Atmos. Chem. Phys.*, 13, 211-224, 10.5194/acp-13-211-
802 2013, 2013a.

803 Sand, M., Berntsen, T. K., Seland, Ø., and Kristjánsson, J. E.: Arctic surface temperature change to
804 emissions of black carbon within Arctic or midlatitudes, *Journal of Geophysical Research:*
805 *Atmospheres*, 118, 7788-7798, 10.1002/jgrd.50613, 2013b.

806 Shindell, D., and Faluvegi, G.: Climate response to regional radiative forcing during the twentieth
807 century, *Nature Geosci*, 2, 294-300,
808 http://www.nature.com/ngeo/journal/v2/n4/supinfo/ngeo473_S1.html, 2009.

809 Shindell, D., Kuylensstierna, J. C. I., Vignati, E., van Dingenen, R., Amann, M., Klimont, Z., Anenberg, S.
810 C., Muller, N., Janssens-Maenhout, G., Raes, F., Schwartz, J., Faluvegi, G., Pozzoli, L., Kupiainen, K.,
811 Hoglund-Isaksson, L., Emberson, L., Streets, D., Ramanathan, V., Hicks, K., Oanh, N. T. K., Milly, G.,
812 Williams, M., Demkine, V., and Fowler, D.: Simultaneously Mitigating Near-Term Climate Change and
813 Improving Human Health and Food Security, *Science*, 335, 183-189, DOI 10.1126/science.1210026,
814 2012.

815 Shindell, D. T., Chin, M., Dentener, F., Doherty, R. M., Faluvegi, G., Fiore, A. M., Hess, P., Koch, D. M.,
816 MacKenzie, I. A., Sanderson, M. G., Schultz, M. G., Schulz, M., Stevenson, D. S., Teich, H., Textor, C.,
817 Wild, O., Bergmann, D. J., Bey, I., Bian, H., Cuvelier, C., Duncan, B. N., Folberth, G., Horowitz, L. W.,
818 Jonson, J., Kaminski, J. W., Marmer, E., Park, R., Pringle, K. J., Schroeder, S., Szopa, S., Takemura, T.,
819 Zeng, G., Keating, T. J., and Zuber, A.: A multi-model assessment of pollution transport to the Arctic,
820 *Atmos. Chem. Phys.*, 8, 5353-5372, 10.5194/acp-8-5353-2008, 2008.

821 Shindell, D. T., Faluvegi, G., Koch, D. M., Schmidt, G. A., Unger, N., and Bauer, S. E.: Improved
822 Attribution of Climate Forcing to Emissions, *Science*, 326, 716-718, 10.1126/science.1174760, 2009.

823 Simpson, D., Benedictow, A., Berge, H., Bergström, R., Emberson, L. D., Fagerli, H., Flechard, C. R.,
824 Hayman, G. D., Gauss, M., Jonson, J. E., Jenkin, M. E., Nyíri, A., Richter, C., Semeena, V. S., Tsyro, S.,
825 Tuovinen, J. P., Valdebenito, Á., and Wind, P.: The EMEP MSC-W chemical transport model –
826 technical description, *Atmos. Chem. Phys.*, 12, 7825-7865, 10.5194/acp-12-7825-2012, 2012.

827 Stamnes, K., Tsay, S. C., Wiscombe, W., and Jayaweera, K.: Numerically Stable Algorithm for Discrete-
828 Ordinate-Method Radiative-Transfer in Multiple-Scattering and Emitting Layered Media, *Appl Optics*,
829 27, 2502-2509, 1988.

830 Stevens, B., and Feingold, G.: Untangling aerosol effects on clouds and precipitation in a buffered
831 system, *Nature*, 461, 607-613, 2009.

832 Stier, P., Schutgens, N. A. J., Bellouin, N., Bian, H., Boucher, O., Chin, M., Ghan, S., Huneeus, N., Kinne,
833 S., Lin, G., Ma, X., Myhre, G., Penner, J. E., Randles, C. A., Samset, B., Schulz, M., Takemura, T., Yu, F.,
834 Yu, H., and Zhou, C.: Host model uncertainties in aerosol radiative forcing estimates: results from the
835 AeroCom Prescribed intercomparison study, *Atmos. Chem. Phys.*, 13, 3245-3270, 10.5194/acp-13-
836 3245-2013, 2013.

837 Stohl, A.: Characteristics of atmospheric transport into the Arctic troposphere, *Journal of Geophysical*
838 *Research: Atmospheres*, 111, n/a-n/a, 10.1029/2005JD006888, 2006.

839 Sudo, K., Takahashi, M., Kurokawa, J.-i., and Akimoto, H.: CHASER: A global chemical model of the
840 troposphere 1. Model description, *Journal of Geophysical Research: Atmospheres*, 107, ACH 7-1-ACH
841 7-20, 10.1029/2001JD001113, 2002.

842 Søvde, O. A., Prather, M. J., Isaksen, I. S. A., Berntsen, T. K., Stordal, F., Zhu, X., Holmes, C. D., and
843 Hsu, J.: The chemical transport model Oslo CTM3, *Geosci. Model Dev.*, 5, 1441-1469, 10.5194/gmd-5-
844 1441-2012, 2012.

845 Takemura, T., Nozawa, T., Emori, S., Nakajima, T. Y., and Nakajima, T.: Simulation of climate response
846 to aerosol direct and indirect effects with aerosol transport-radiation model, *Journal of Geophysical
847 Research: Atmospheres*, 110, n/a-n/a, 10.1029/2004JD005029, 2005.

848 Textor, C., Schulz, M., Guibert, S., Kinne, S., Balkanski, Y., Bauer, S., Berntsen, T., Berglen, T., Boucher,
849 O., Chin, M., Dentener, F., Diehl, T., Feichter, J., Fillmore, D., Ginoux, P., Gong, S., Grini, A., Hendricks,
850 J., Horowitz, L., Huang, P., Isaksen, I. S. A., Iversen, T., Kloster, S., Koch, D., Kirkevåg, A., Kristjansson,
851 J. E., Krol, M., Lauer, A., Lamarque, J. F., Liu, X., Montanaro, V., Myhre, G., Penner, J. E., Pitari, G.,
852 Reddy, M. S., Seland, Ø., Stier, P., Takemura, T., and Tie, X.: The effect of harmonized emissions on
853 aerosol properties in global models – an AeroCom experiment, *Atmos. Chem. Phys.*, 7, 4489-4501,
854 10.5194/acp-7-4489-2007, 2007.

855 Tiedtke, M.: A Comprehensive Mass Flux Scheme for Cumulus Parameterization in Large-Scale
856 Models, *Monthly Weather Review*, 117, 1779-1800, 10.1175/1520-
857 0493(1989)117<1779:ACMFSF>2.0.CO;2, 1989.

858 Tilmes, S. L., J.-F.; Emmons, L.K.; Kinnison, D.E.; Marsh, D.; Garcia, R.R.; Smith, A.K.; Neely, R.R.;
859 Conley, A.; Vitt, F.; Val Martin, M.; Tanimoto, H.; Simpson, I.; Blake, D.R.; Blake, N.: Representation of
860 the Community Earth System Model (CESM1) CAM4-chem within the Chemistry-ClimateModel
861 Initiative (CCMI), Accepted for publication in *Geosci. Model Dev.*, 2016, 1-50, 10.5194/gmd-2015-
862 237, 2016.

863 Tsigaridis, K., Daskalakis, N., Kanakidou, M., Adams, P. J., Artaxo, P., Bahadur, R., Balkanski, Y., Bauer,
864 S. E., Bellouin, N., Benedetti, A., Bergman, T., Berntsen, T. K., Beukes, J. P., Bian, H., Carslaw, K. S.,
865 Chin, M., Curci, G., Diehl, T., Easter, R. C., Ghan, S. J., Gong, S. L., Hodzic, A., Hoyle, C. R., Iversen, T.,
866 Jathar, S., Jimenez, J. L., Kaiser, J. W., Kirkevåg, A., Koch, D., Kokkola, H., Lee, Y. H., Lin, G., Liu, X., Luo,
867 G., Ma, X., Mann, G. W., Mihalopoulos, N., Morcrette, J. J., Müller, J. F., Myhre, G., Myriokefalitakis,
868 S., Ng, N. L., O'Donnell, D., Penner, J. E., Pozzoli, L., Pringle, K. J., Russell, L. M., Schulz, M., Sciare, J.,
869 Seland, Ø., Shindell, D. T., Sillman, S., Skeie, R. B., Spracklen, D., Stavrou, T., Steenrod, S. D.,
870 Takemura, T., Tiitta, P., Tilmes, S., Tost, H., van Noije, T., van Zyl, P. G., von Salzen, K., Yu, F., Wang, Z.,
871 Wang, Z., Zaveri, R. A., Zhang, H., Zhang, K., Zhang, Q., and Zhang, X.: The AeroCom evaluation and
872 intercomparison of organic aerosol in global models, *Atmos. Chem. Phys.*, 14, 10845-10895,
873 10.5194/acp-14-10845-2014, 2014.

874 Vuolo, M. R., Schulz, M., Balkanski, Y., and Takemura, T.: A new method for evaluating the impact of
875 vertical distribution on aerosol radiative forcing in general circulation models, *Atmos. Chem. Phys.*,
876 14, 877-897, 10.5194/acp-14-877-2014, 2014.

877 Watanabe, M., Suzuki, T., O'ishi, R., Komuro, Y., Watanabe, S., Emori, S., Takemura, T., Chikira, M.,
878 Ogura, T., Sekiguchi, M., Takata, K., Yamazaki, D., Yokohata, T., Nozawa, T., Hasumi, H., Tatebe, H.,
879 and Kimoto, M.: Improved Climate Simulation by MIROC5: Mean States, Variability, and Climate
880 Sensitivity, *Journal of Climate*, 23, 6312-6335, 10.1175/2010JCLI3679.1, 2010.

881 Wilcox, L. J., Highwood, E. J., Booth, B. B. B., and Carslaw, K. S.: Quantifying sources of inter-model
882 diversity in the cloud albedo effect, *Geophysical Research Letters*, 42, 1568-1575,
883 10.1002/2015GL063301, 2015.

884 Wu, S., Mickley, L. J., Jacob, D. J., Logan, J. A., Yantosca, R. M., and Rind, D.: Why are there large
885 differences between models in global budgets of tropospheric ozone?, *Journal of Geophysical*
886 *Research: Atmospheres*, 112, n/a-n/a, 10.1029/2006JD007801, 2007.

887 Yu, H., Kaufman, Y. J., Chin, M., Feingold, G., Remer, L. A., Anderson, T. L., Balkanski, Y., Bellouin, N.,
888 Boucher, O., Christopher, S., DeCola, P., Kahn, R., Koch, D., Loeb, N., Reddy, M. S., Schulz, M.,
889 Takemura, T., and Zhou, M.: A review of measurement-based assessments of the aerosol direct
890 radiative effect and forcing, *Atmos. Chem. Phys.*, 6, 613-666, 10.5194/acp-6-613-2006, 2006.

891 Yu, H., Remer, L. A., Chin, M., Bian, H., Tan, Q., Yuan, T., and Zhang, Y.: Aerosols from Overseas Rival
892 Domestic Emissions over North America, *Science*, 337, 566-569, 10.1126/science.1217576, 2012.

893 Yu, H. B., Chin, M., West, J. J., Atherton, C. S., Bellouin, N., Bergmann, D., Bey, I., Bian, H. S., Diehl, T.,
894 Forberth, G., Hess, P., Schulz, M., Shindell, D., Takemura, T., and Tan, Q.: A multimodel assessment of
895 the influence of regional anthropogenic emission reductions on aerosol direct radiative forcing and
896 the role of intercontinental transport, *Journal of Geophysical Research-Atmospheres*, 118, 700-720,
897 2013.

898 Zarzycki, C. M., and Bond, T. C.: How much can the vertical distribution of black carbon affect its
899 global direct radiative forcing?, *Geophysical Research Letters*, 37, n/a-n/a, 10.1029/2010GL044555,
900 2010.

901 Zhang, G. J., and McFarlane, N. A.: Sensitivity of climate simulations to the parameterization of
902 cumulus convection in the Canadian climate centre general circulation model, *Atmosphere-Ocean*,
903 33, 407-446, 1995.

904 Zhang, K., Wan, H., Liu, X., Ghan, S. J., Kooperman, G. J., Ma, P. L., Rasch, P. J., Neubauer, D., and
905 Lohmann, U.: Technical Note: On the use of nudging for aerosol-climate model intercomparison
906 studies, *Atmos. Chem. Phys.*, 14, 8631-8645, 10.5194/acp-14-8631-2014, 2014.

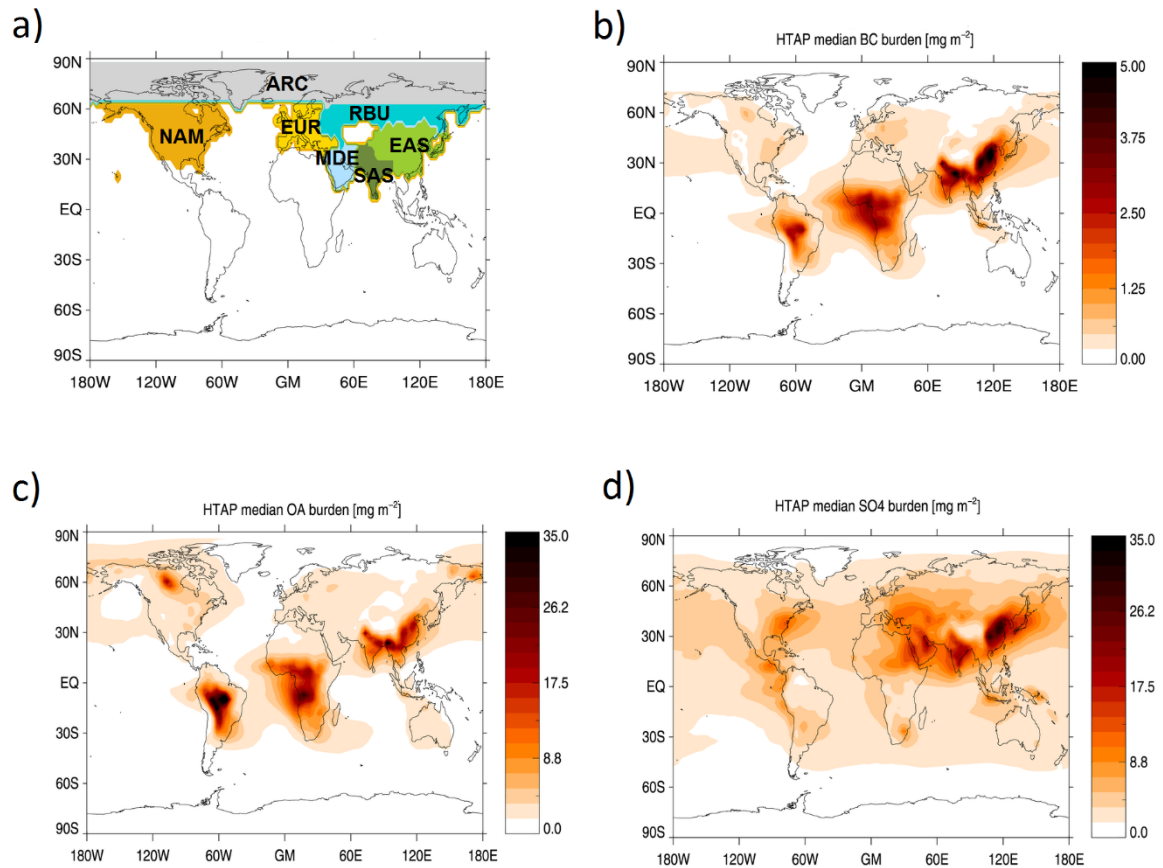
907

908 **Figures**

909

910

911

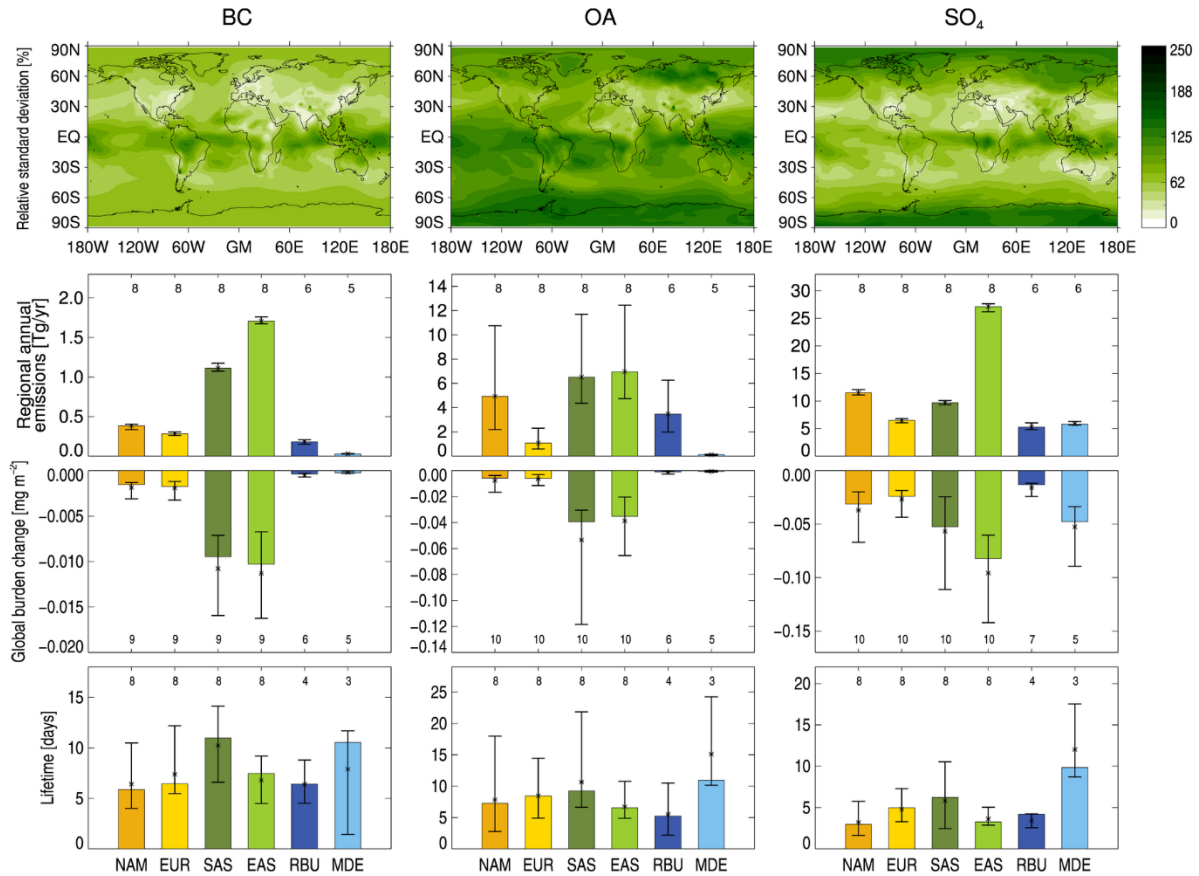


912

913

914

915 **Figure 1:** a) Regions of focus (NAM: North America; EUR: Europe; EAS: East Asia; SAS: South Asia; RBU;
916 Russia/Belarus/Ukraine, MDE: Middle East and ARC: Arctic). b), c) and d) show multi-model median
917 (calculated at each grid point), annual mean aerosol load of the *BASE* experiment for BC, OA and SO₄,
918 respectively.

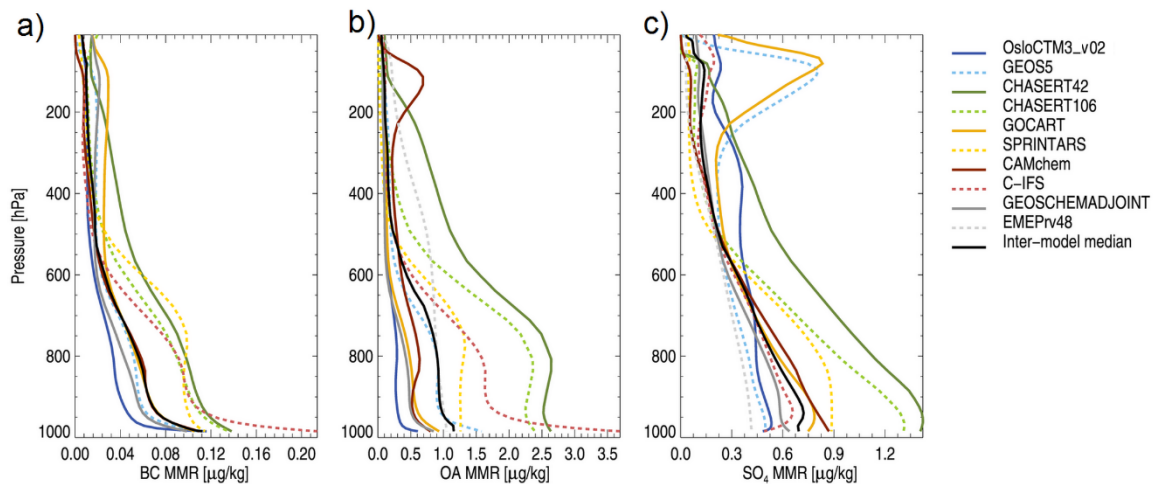


920 **Figure 2:** Top row: Relative inter-model standard deviation in annual mean aerosol emissions. Second row: Regionally
 921 averaged annual mean aerosol emissions (for SO₄, we give SO₂ emissions, in Tg SO₂), for the source regions shown in Fig. 1.
 922 Numbers are from the *BASE* simulations. Error bars show the maximum and minimum emissions for the sample of models
 923 used here, and the numbers above the bars give the number of models that have data for the given value. Third row: Globally
 924 and annually averaged aerosol burden change for 20 % emission reductions in the indicated region. Numbers are from the
 925 perturbation simulations. Bottom row: Aerosol lifetime, here defined as the global change in burden divided by the global
 926 change in emissions following an emission reduction within a given source region (see main text, Eq. 4).
 927

928

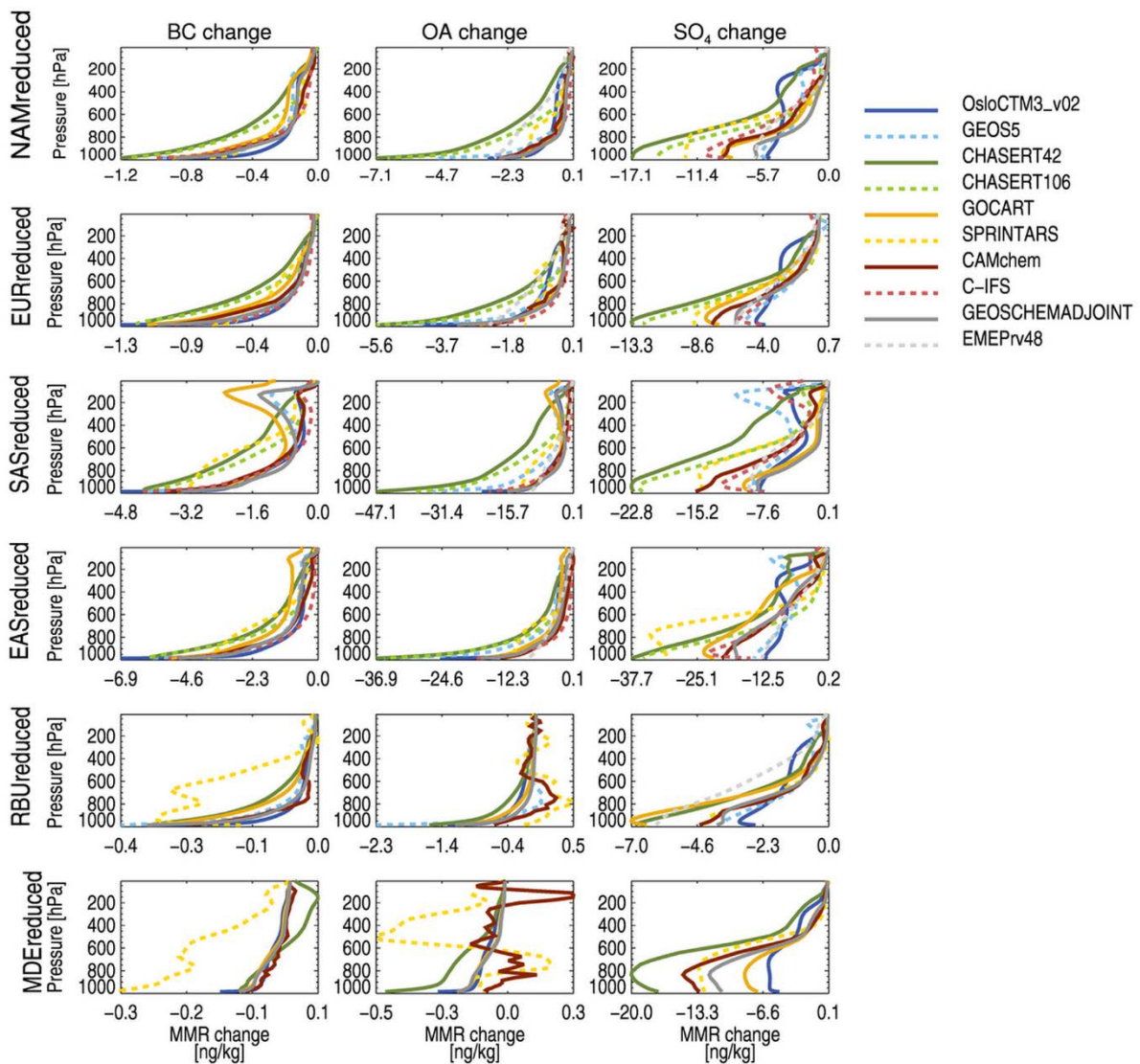
929

930



931 **Figure 3:** Globally and annually averaged mass mixing ratios (MMR) of a) BC, b) OA and c) SO₄, for all contributing
 932 models for the *BASE* experiment.
 933
 934
 935

936
937
938
939



940

941

942 **Figure 4:** Globally averaged change in MMR per model layer, when reducing emissions by 20 % within the region indicated
943 (rows), for all aerosol species (columns). Each line represents one model. See Tables S-2 to S-4 for the total burden changes
944 for all models, experiments and species.

945

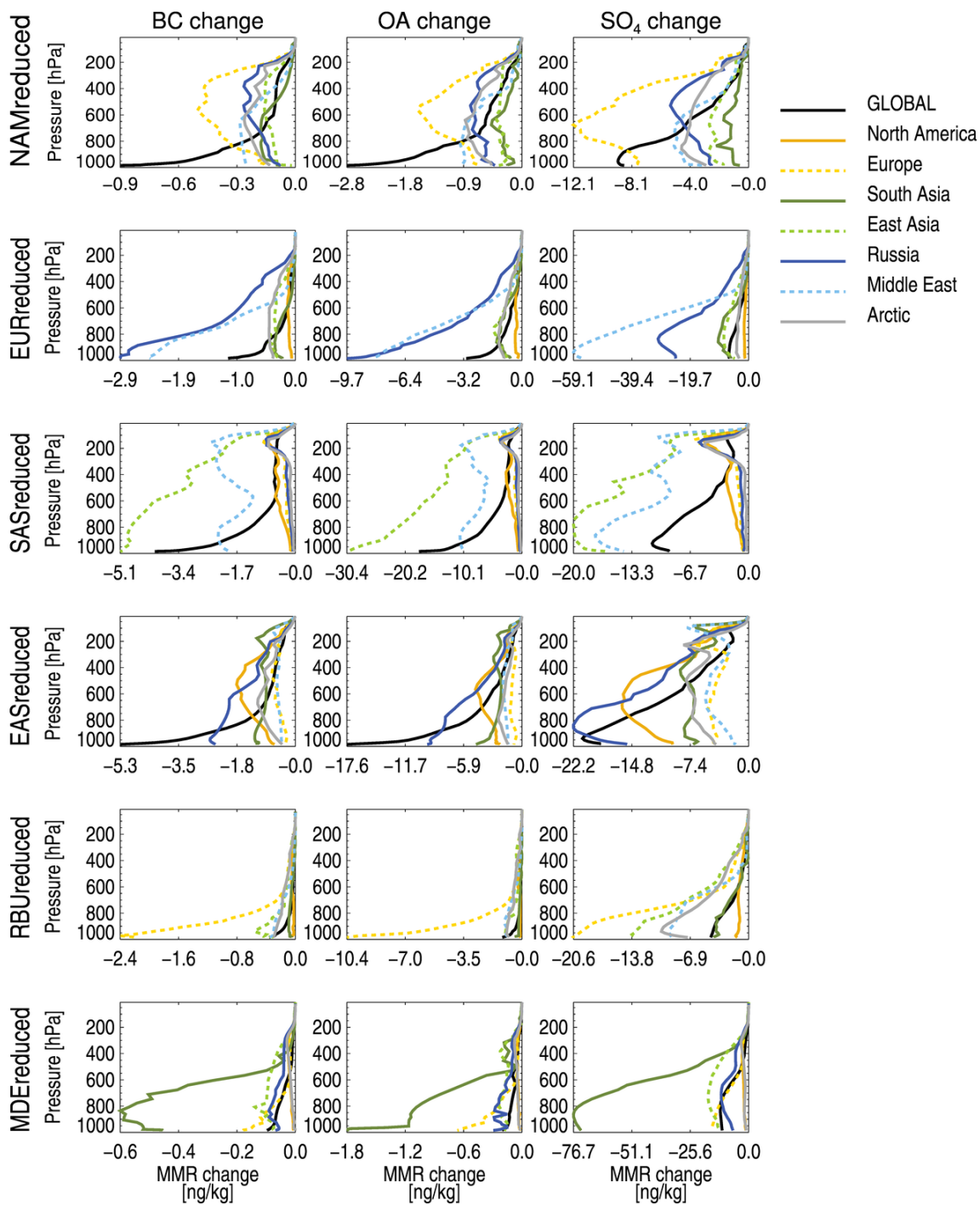
946

947

948

949

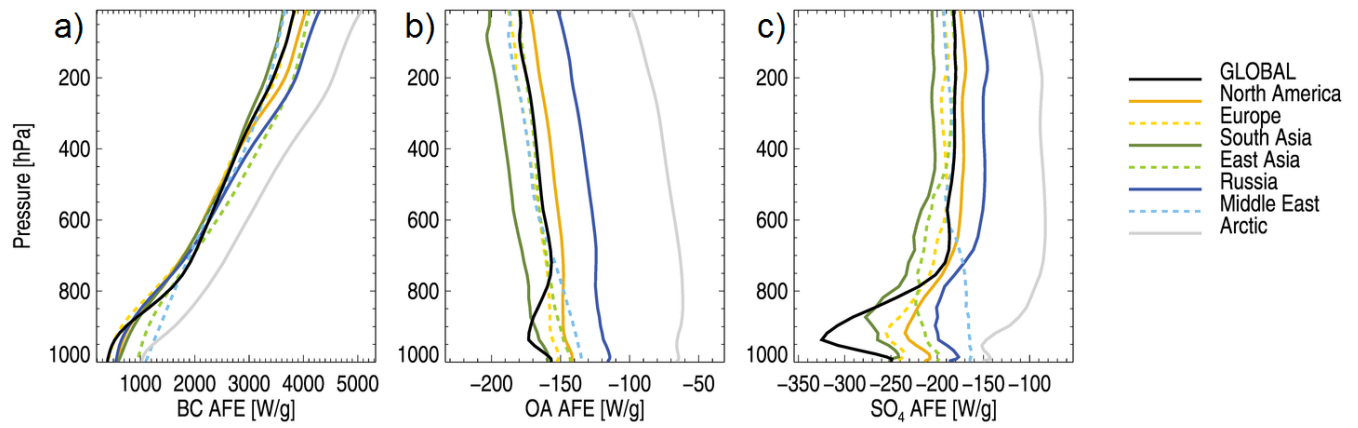
950



951

952 **Figure 5:** Model-averaged aerosol MMR change profiles for different receptor regions (marked by the colors of the lines),
 953 for emission reductions in the six source regions (rows) and for BC (first column), OA (middle column) and SO₄ (last
 954 column).

955

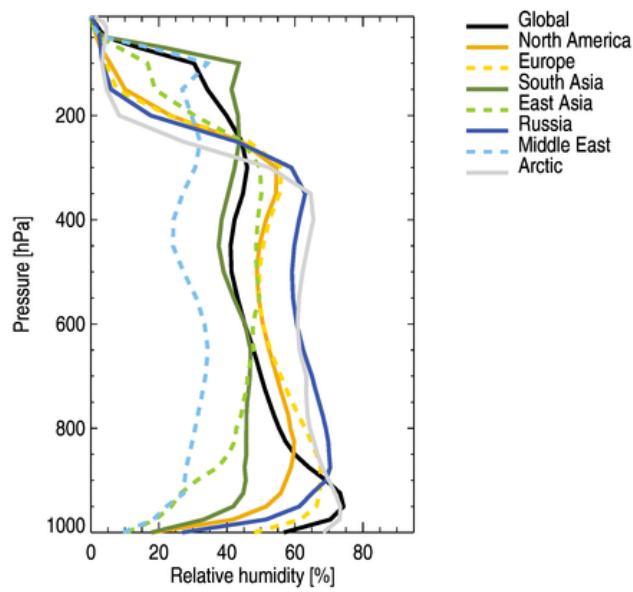


956

957

958 **Figure 6:** Aerosol forcing efficiency profiles, i.e. TOA radiative forcing exerted per gram of aerosol versus altitude,
 959 calculated by the OsloCTM2 model. Black, solid lines indicate global, annual mean profiles. Colored lines show the annual
 960 mean profiles within the regions of Figure 1a.

961

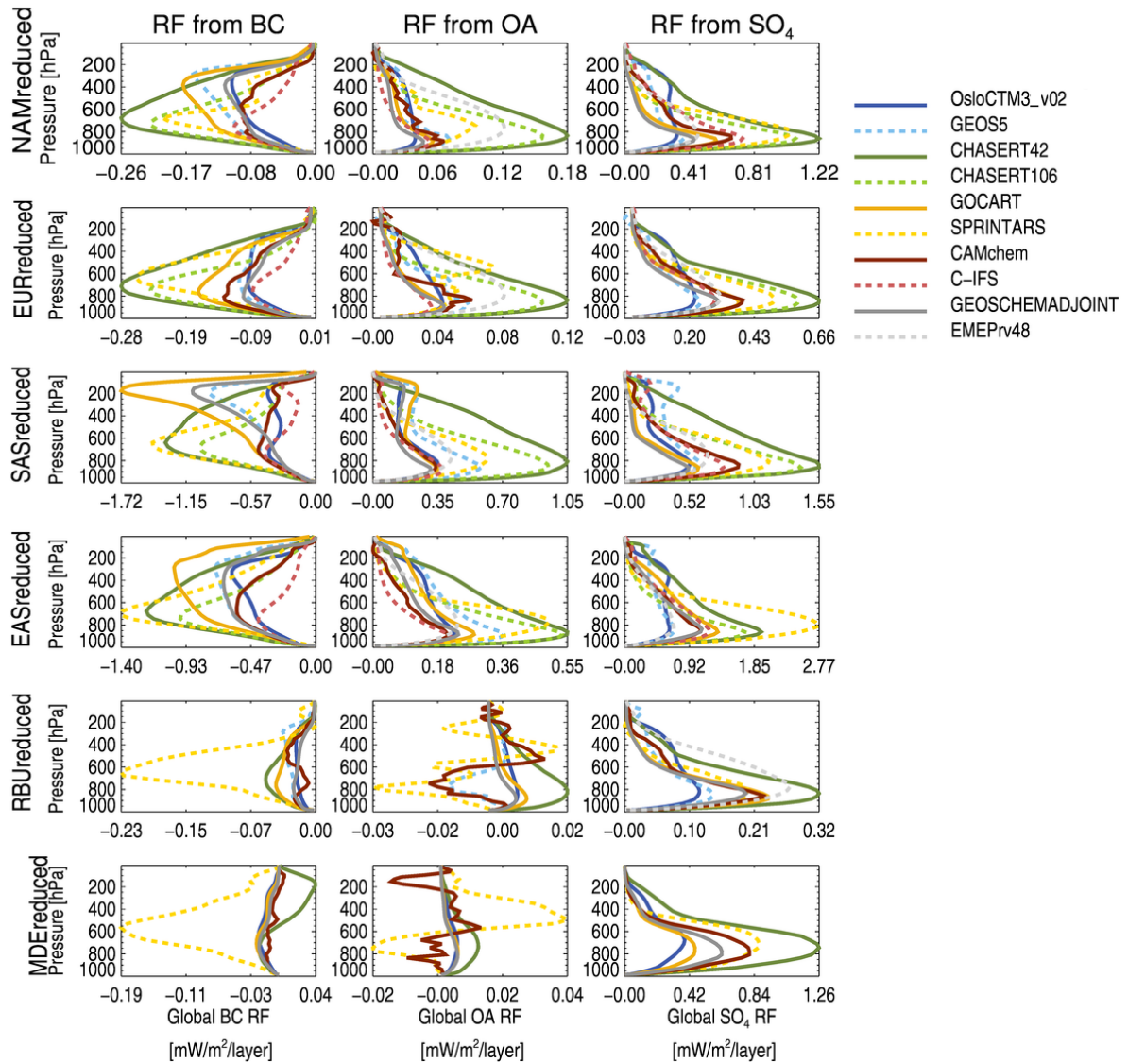


962

963 **Figure 7:** Annually averaged relative humidity from MERRA data, for year 2010, for the same regions as in Figure 6.

964

965

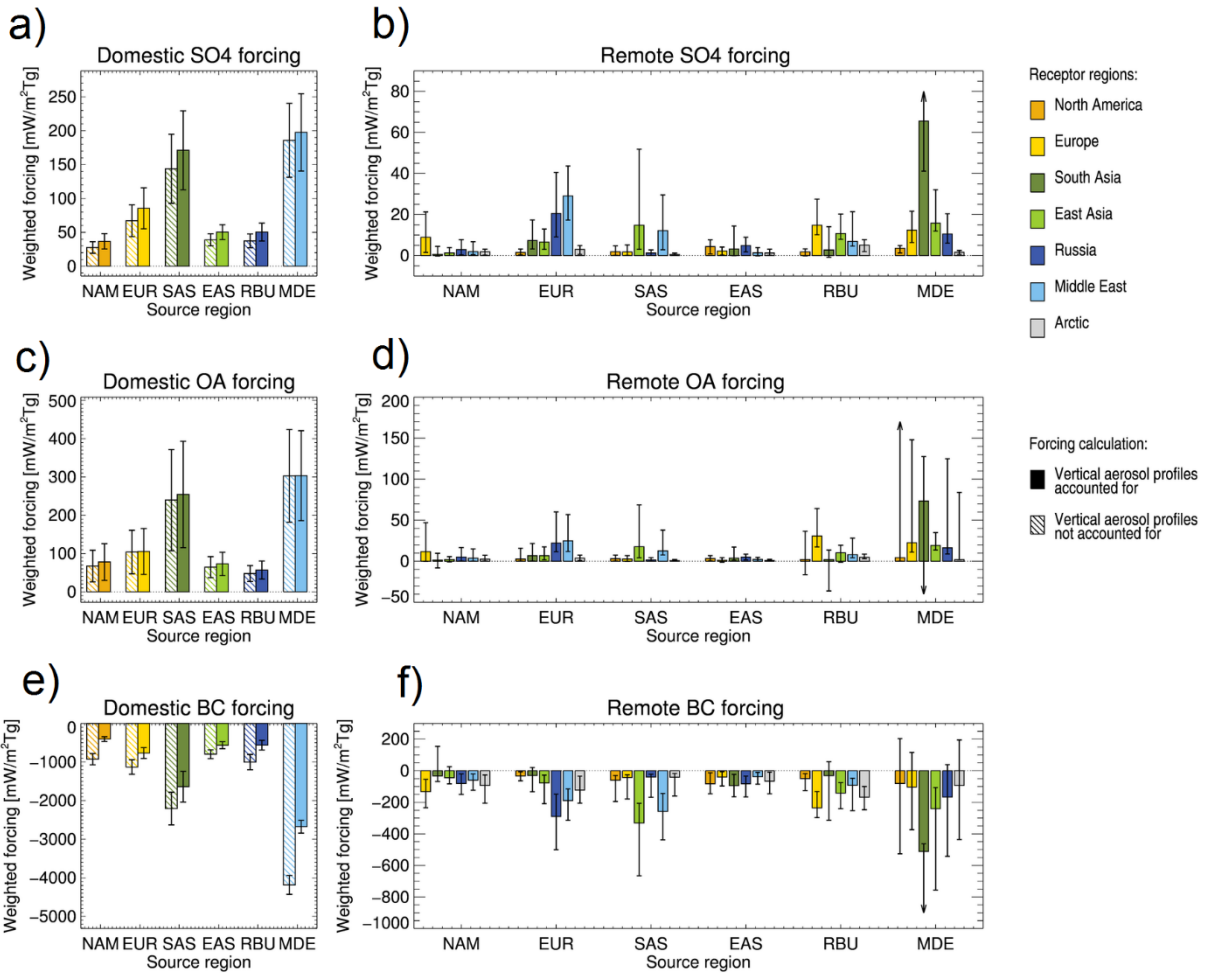


967

968 **Figure 8:** Global mean vertically resolved aerosol direct radiative forcing, when reducing emissions by 20 % within the
 969 region indicated (rows), for all aerosol species (columns). Each line represents one model. See Tables S-2 to S-4 for
 970 individual model results.

971

972



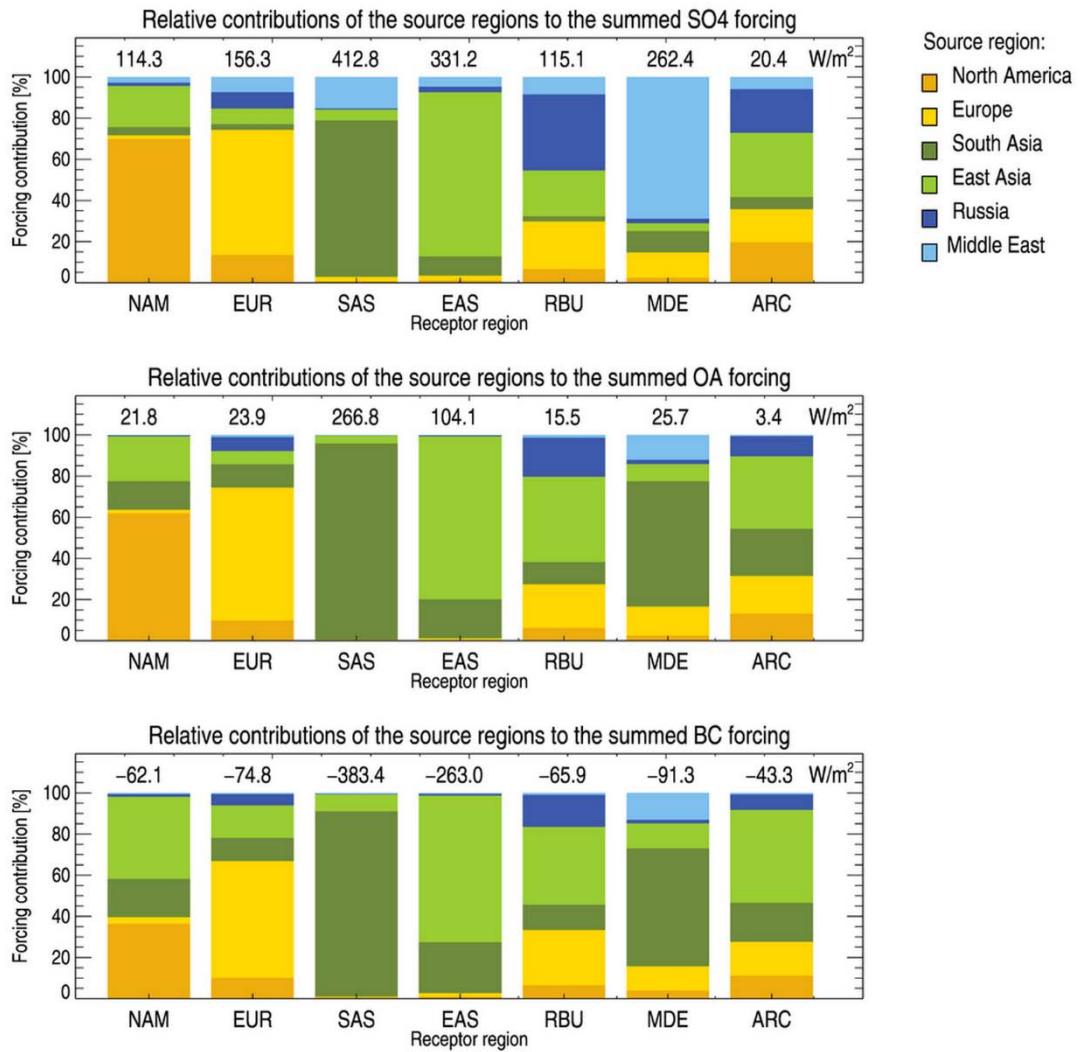
973

974 **Figure 9:** Regionally averaged forcing in the six source regions due to domestic emission reductions (leftmost column) and
 975 remote forcings averaged over different receptor regions due to emission reductions in the six source regions (rightmost
 976 column) for the three aerosol species (top row: SO₄; middle row: OA; lower row: BC). Forcings are weighed by the emission
 977 change in each given source region. The source region in question is marked on the x axis, while the receptor region for
 978 which the forcing is averaged is marked by the color of the bar. See Tables S-6 through S-8 for the numbers behind this
 979 figure.

980

981

982



983

984 **Figure 10:** Relative contributions of the individual source regions (colors on the bars) to the summed forcing, averaged over
 985 each of the receptor regions (given on the x axis and seen in Fig. 1 (a)). The summed forcing that the given receptor region
 986 experiences due to emission-reductions in the six source regions is given in numbers above each bar.

987

988

989

Tables

Table 1: Models used for the present study, with relevant information and references.

	Version	Horizontal resolution	Vert. layers	Meteorology input source	Convection	Reference
SPRINTARS	atmosphere: MIROC5.2	1.1° x 1.1°	56	ECMWF Interim.	The cumulus scheme (Chikira and Sugiyama, 2010) is an entraining plume model, in which the lateral entrainment rate varies vertically depending on the surrounding environment. The cloud base mass flux is determined with a prognostic convective kinetic energy closure.	Watanabe et al. (2010) Takemura et al. (2005)
OsloCTM3_v02	v02, all aerosol modules from OsloCTM2	2.8° x 2.8°	60	ECMWF's Integrated Forecast System (IFS) model	The parameterization of deep convection is based on the Tiedke mass flux scheme (Tiedtke, 1989).	Søvde et al. (2012)
GOCART	v5 2010	1.3° x 1.0°	72	MERRA	Moist convection is parameterized using archived cloud mass flux fields from MERRA. GCTM convection is parameterized using cloud mass flux information from the relaxed Arakawa-Schubert (RAS) algorithm (Moorthi and Suarez, 1992).	Chin et al. (2000)
C-IFS	IFS CY40r2	0.7° x 0.7°	54	Relaxed to ERA-Interim	Tiedtke (1989) shallow convection scheme.	Flemming et al. (2015)
CHASER-T42	v4.0, MIROC-ESM version	2.8° x 2.8°	32	ERA-Interim (u,v,T) and HadISST	Transport due to advection, convection, and other subgrid-scale mixing are simulated “on-line” by the dynamical component of the CCSR/NIES AGCM. The prognostic Arakawa-Schubert scheme is employed to simulate cumulus convection.	Sudo et al. (2002)
CHASER-T106	v4.0, MIROC-ESM version	1.1° x 1.1°	32	(as above)	(as above)	Sudo et al. (2002)
CAMchem	CESM1-CAM4-chemSD	1.9° x 2.5°	56	GEOS5 v5.2 meteorology	Deep convection is parameterized using the Zhang-McFarlane approach (Zhang and McFarlane, 1995), with some modifications, while shallow convection follows Hack et al. (2006)	Tilmes (2016)
GEOS5	v5	1.3° x 1.0°	72	MERRA	Convection is based on a modified version of the scheme described by Moorthi and Suarez (1992), which is a relaxed Arakawa-Schubert algorithm (RAS).	Rienecker et al. (2008) Colarco et al. (2010)
GEOSCHEMADJOINT	v35f	2.0° x 2.5°	47	GEOS-5 (MERRA)	Convective transport in GEOS Chem is computed from the convective mass fluxes in the meteorological archive, as described by Wu et al. (2007), which is taken from GEOS-5 (see above).	Henze et al. (2007)
EMEPv48	rv4.8	0.5° x 0.5°	20	ECMWF's Integrated Forecast System (IFS) model	(see OsloCTM3_v02 above)	Simpson et al. (2012)

Table 2: Regionally averaged burdens and climatological features for the six source regions. Burdens are multi-model median, annually averaged values for the *BASE* experiment with one multi-model standard deviation in parenthesis. Convective mass flux (for the layers between 1000 and 500 hPa), precipitation and cloud cover represent regionally and annually averaged values for 2010 from the Modern-Era Retrospective analysis for Research and Applications (MERRA) reanalysis data set.

	Region name	BC burden [mgm ⁻²]	OA burden [mgm ⁻²]	SO₄ burden [mgm ⁻²]	Convective mass flux [kgm⁻²]	Precipitation [mm/day]	Cloud cover [%]
NAM	North America	0.36 (± 0.09)	3.86 (± 3.45)	3.55 (± 1.28)	3980	1.92	55
EUR	Europe	0.39 (± 0.09)	2.70 (± 1.83)	5.44 (± 1.43)	4774	1.89	53
SAS	South Asia	1.85 (± 0.36)	14.57 (± 7.67)	11.34 (± 3.57)	9769	3.34	43
EAS	East Asia	1.25 (± 0.26)	7.48 (± 4.17)	9.16 (± 2.43)	4105	1.89	46
RBU	Russia	0.29 (± 0.09)	2.84 (± 2.71)	4.58 (± 2.05)	2741	1.44	63
MDE	Middle East	0.41 (± 0.12)	3.43 (± 3.53)	11.54 (± 3.48)	1247	0.41	23

Table 3: Globally averaged radiative forcing from the six main experiments, weighed by the emission change for the given source region. Relative one standard deviations (representing multi-model variation) are given in parentheses.

	BC [mWm ⁻² Tg ⁻¹]	OA [mWm ⁻² Tg ⁻¹]	SO₄ [mWm ⁻² Tg ⁻¹]
NAMreduced	51.9 (± 0.4)	-7.9 (± 0.8)	-4.5 (± 0.5)
EURreduced	55.2 (± 0.4)	-6.8 (± 0.6)	-5.6 (± 0.4)
SASreduced	93.8 (± 0.4)	-10.2 (± 0.6)	-7.9 (± 0.5)
EASreduced	54.5 (± 0.3)	-5.1 (± 0.5)	-4.4 (± 0.3)
RBUreduced	78.3 (± 0.6)	-2.4 (± 2.2)	-3.6 (± 0.3)
MDEreduced	201.8 (± 1.6)	-17.9 (± 0.4)	-10.3 (± 0.7)

Table 4: Response to Extra-Regional Emission Reductions (RERER), averaged over the 10 participating models, \pm one standard deviation representing inter-model spread. A high RERER value means that the given region is very sensitive to extra-regional emission reductions. The top table shows RERER for column aerosol burdens, the bottom table shows RERER for direct radiative forcing (DRF) calculated using vertically, spatially and temporally resolved AFE profiles.

Burden change	NAM	EUR	SAS	EAS	RBU	MDE
BC	0.51 \pm 0.13	0.37 \pm 0.06	0.12 \pm 0.03	0.21 \pm 0.05	0.83 \pm 0.04	0.87 \pm 0.04
OA	0.49 \pm 0.19	0.41 \pm 0.08	0.09 \pm 0.03	0.24 \pm 0.06	0.82 \pm 0.06	0.90 \pm 0.06
SO₄	0.46 \pm 0.14	0.54 \pm 0.09	0.36 \pm 0.04	0.32 \pm 0.07	0.75 \pm 0.06	0.46 \pm 0.08
DRF	NAM	EUR	SAS	EAS	RBU	MDE
BC	0.69 \pm 0.11	0.57 \pm 0.10	0.18 \pm 0.04	0.37 \pm 0.06	0.89 \pm 0.03	0.91 \pm 0.03
OA	0.46 \pm 0.18	0.46 \pm 0.08	0.09 \pm 0.02	0.27 \pm 0.06	0.83 \pm 0.07	0.91 \pm 0.06
SO₄	0.41 \pm 0.12	0.53 \pm 0.08	0.34 \pm 0.04	0.31 \pm 0.07	0.73 \pm 0.05	0.47 \pm 0.08